Design of Functional Polymer Hybrid Hydrogels Based on Imogolite and Halloysite Clay Nanotubes

朴，景麟

Design of Functional Polymer Hybrid Hydrogels Based on Imogolite and Halloysite Clay Nanotubes

イモゴライトとハロイサイトナノチューブを用いた機能性ポリマーハイブリッドハイドロゲルの設計

July 2017

Kyung-Lynne Park

Table of Contents

Chapter 1 General Introduction

Chapter 2 Effect of Imogolite Nanotubes as Nano-fillers on Hyaluronic Acid Hybrid Hydrogels

Chapter 3 Hybrid Hydrogels Based on Halloysite Nanotubes and Hyaluronic Acid

Chapter 4 Drug Nanocarriers Based on pH Sensitive Halloysite Nanotubes

Chapter 1

General Introduction

1.1 Clay nanotubes

Clay minerals are defined as hydrated phyllosilicates (sheet silicates) consisting of the fine-grained fraction of rocks, sediments, and soils, which impart plasticity to clay and harden upon drying or firing.[1] Among them, halloysite, imogolite and chrysotile are representative examples of naturally occurring clay minerals with tubular structures (Figure 1-1). Their unique structure and chemical properties make them useful in several industrial fields. However, chrysotile is regarded as a type of asbestos which have health risk issues, and it is restrictive in its use. Unlike chrysotile, imogolite and halloysite is much safer in health risk aspect, which make it possible in numerous industrial applications as a nanotube material.[2] Synthetic nanotubes, e.g. carbon nanotubes and inorganic nanotubes including MoS_2, WS_2, and TiS_2 have found important applications such as catalysis, electronics, polymer nanocomposites, adsorption and sensing applications.[3-5] However, time-consuming preparation and small amount production of nanotubes lead to high material costs and, consequently, limit their actual applications. In contrast, Halloysite and Imogolite can be good candidates as industrial advanced nanotube materials because of their interesting properties such as large specific surface area, high surface reactivity and mechanical strength, low cost, and, moreover, environmentally friendly green materials.[2]

Nanocomposites are multiphase solid materials where they contain at least one of the phases with nano-scale domain. The most attractive thing about nanocomposite is that they show synergistic properties which are significantly different from those of the individual components. Small amounts of clay minerals dispersed in a polymer matrix can enhance the performance of the polymers in the clay-based polymer nanocomposites. For the last several decades, most of the nanocomposite researches were mostly devoted

to the 2:1 phyllosilicates comprising the smectite clays. However, clay nanotubes such as halloysite, 1:1 phyllosilicate, and imogolite have been intensively studied in polymer nanocomposite technology recently. One of the major challenges to optimize the performance of the polymer nanocomposites are to obtain the highest aspect ratio of the dispersed nanoparticles in the polymer matrix i.e. exfoliated nanocomposites. There are three representative dispersion models in clay-based polymer nanocomposites (CPN) (Figure 1-2).[6] In particular, the interfacial interaction between the clay minerals and polymer matrix as well as the nature and structure of the clay mineral should be considered to design the CPN because these factors play a vital role in the enhancement of the desired properties. From this point of view, highly surface active clay nanotubes can be the prospective nano-scale materials to shed a bright light on CPN development.
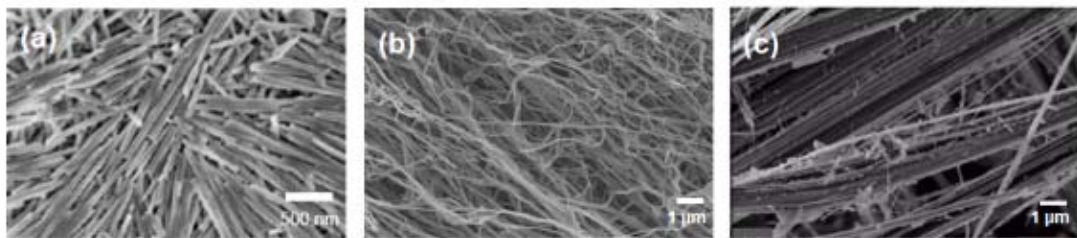
Figure 1-1. FE-SEM image of clay nanotubes: (a) Halloysite, (b) Imogolite, (c) Chrysotile.[7]
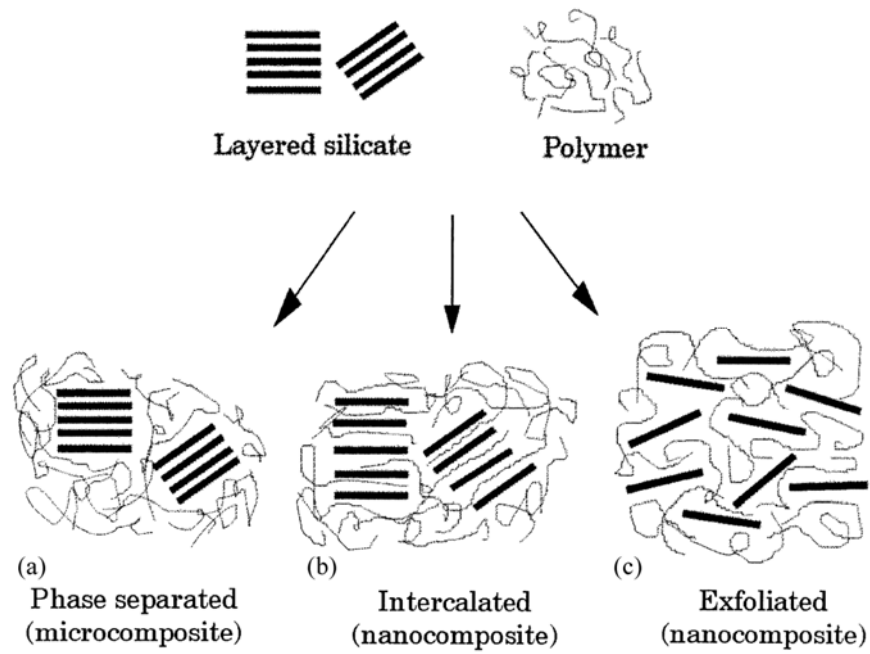
Figure 1-2. Schematic of representative dispersion state of clay mineral nanoparticles in polymer

matrix.[6]

1.2 Imogolite and halloysite nanotubes

Imogolite is a hydrous aluminosilicate material with the composition of $(OH)_3Al_2O_3SiOH$ (Figure 1-3). Imogolite has a hollow nanotubular structure with an external diameter of ca. 2 - 2.5 nm and an internal diameter of less than 1 nm, resulted from a curling of the gibbsite-like sheet. Imogolite has high aspect ratio and large surface area with length ranging from sub to several micrometers. The outer and inner surface of imogolite is composed of Al-OH groups and Si-OH groups, respectively. The charge density of imogolite surface varies with ionic strength of solvent since Al-OH and Si-OH are protonated. The dispersity of imogolite in water changes dramatically depending on the pH, i.e. imogolite disperses as monofilament or thin bundle in acidic water (below pH 5) due to the electrostatic repulsion of charged surface. In contrast, imogolite assembles into thick bundle or network with an increase of pH.[8-11] The high surface area and remarkable surface chemistry makes this nanotube very attractive for biomedical applications. Imogolite/DNA and fish gelatin gels were developed for potential biomedical applications (Figure 1-4).[12,13] Also, imogolite was evaluated that it has good cytocompatibility in osteoblast-like cell culture .[14]
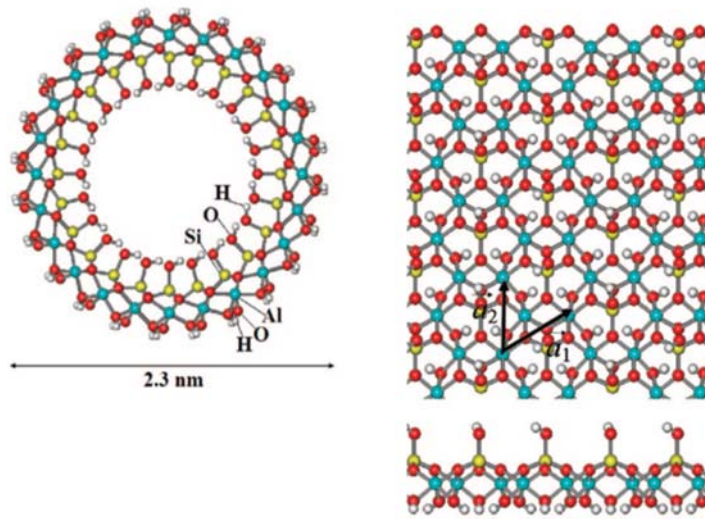
Figure 1-3. Schematic illustration of Imogolite nanotube structure. White atoms, H; red, O; blue, Al; yellow, Si.[15]

(a)　　　　　　　　　　　　　　　　　　　(b)
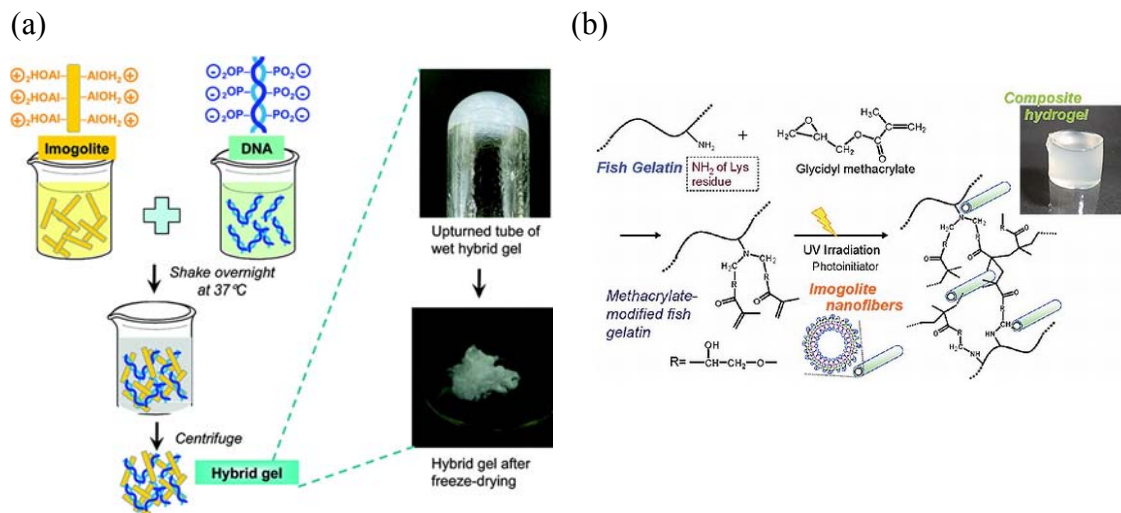
Figure 1-4. Schematic illustration of Bioapplication of imogolite nanotubes: (a) Imogolite/DNA hybrid hydrogels.[12] (b) Imogolite/Fish Gelatin hybrid hydrogels.[13]

Halloysite is a naturally occurring green material and its aluminosilicate sheets are rolled into tubes. The remarkable feature of halloysite is the different surface chemistry at inner and outer sides of the tube. The outer silica surface is charged negatively and the inner alumina surface is charged positively in pH range of 2 – 9. The wall consists of 1-15 bilayers of aluminum and silicon oxide. Halloysite dimensions vary depending on the deposit. Generally, They have an aspect ratio of *ca.*20 and a length of 0.2-1.5 μm. Outer and inner diameter is in the ranges of 40-70 nm and 10-30 nm, respectively (Figure 1-5). This unique bivalent morphology and large specific surface area makes halloysite nanotube a promising biomaterials for drug delivery and tissue scaffolds.[16-17] The inner side of aluminol groups can be easily modified by organophosphonic acid and, subsequently, hydrophobic molecule can interact with the inner lumen. Furthermore, outside silanol groups can be further modified by silane coupling agent resulting in bifunctionalized HNTs (Figure 1-6).[19]
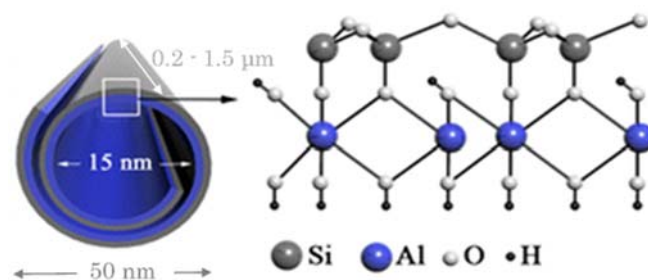
Figure 1-5. Schematic illustration of halloysite nanotubes structure (HNTs).[18]
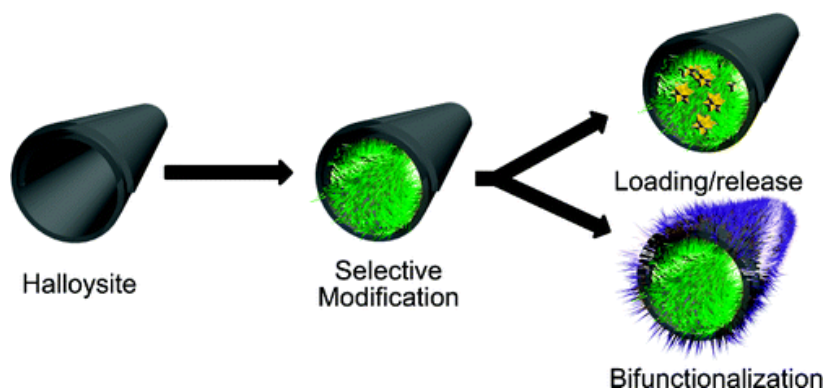
Figure 1-6. Schematic illustration of the loading and releasing of organic compound, and bifunctionalization of halloysite nanotubes (HNTs).[19]

1.3 Clay-based hybrid hydrogels

Great attention has been paid to the hydrogels for their unique properties such as capacity of absorbing and maintaining high water content, highly porous structure, viscoelasticity, good bioadhesivity and biocompatibility, and biodegradability to safe products.[20-27] Therefore, hydrogels have been actively used in energy & environmental area[22,28,29], and biomedical applications including regenerative medicine,[30-32] drug delivery,[33-35] and diagnostics.[36,37]

Nanocomposite hydrogels are hydrated polymeric networks either physically or chemically cross-linked with each other and/ or with nanoparticles or nanostructure. They have superior physical, chemical, electrical and biological properties compared to the conventional polymeric hydrogels. Recently, nanocomposite hydrogels have been extensively studied because they present the synergistic effect by combining advantageous components with different physicochemical properties in hydrogels. Especially, they have been widely used in biomedical application such as tissue engineering, drug delivery, and biomedical devices. There can be divided into 4 types of nanocomposite hydrogels based on carbon-based nanomaterials, polymeric nanoparticles, inorganic nanoparticles, and metal/metal-oxide nanoparticles (Figure 1-7).[38,39]
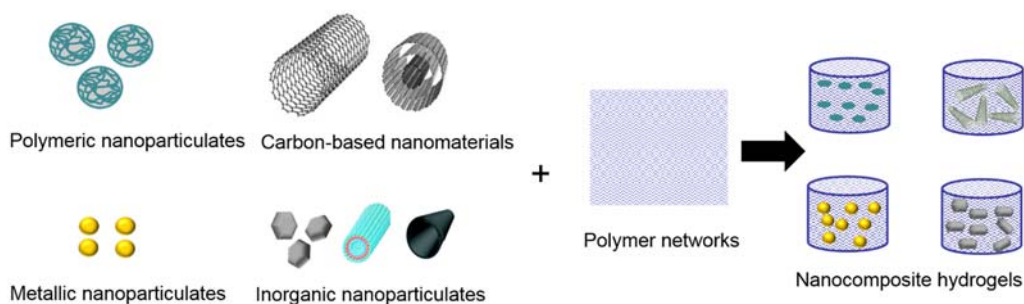
Figure 1-7. Schematic illustration of a type of engineered nanocomposite hydrogels

Nanocomposite hydrogels have been developed to substitute and repair biological tissues. Among these, several new attempts have been extensively made on designing self-assembled and smart nanocomposite hydrogels that respond to external stimuli such as optic, temperature, mechanical, electric and magnetic fields. The sensitivity of these hydrogels to external stimuli is very important for the design of smart implants and drug delivery systems as well as new bio-technologies including biosensors, actuators, *in vitro* diagnostics, cell culture matrixes, contrast agents and bioassays.[40-42]

A variety of clay-based nanocomposite hydrogels are fabricated by the combination of inorganic nanoparticles with synthetic or natural origin polymers. Silicate nanoparticles (clay) have been extensively used to improve the mechanical properties of synthetic and natural polymers. The resulting clay-based nanocomposite hydrogels often show significant improvements in structure, modulus, strength and toughness, of which properties cannot be achieved by using the polymer hydrogel alone. Thus, polymers commonly used for biomedical applications have been reinforced by the addition of silicate nanoparticles. Clay minerals can be used as fillers or cross-linkers to improve the mechanical properties of polymer hydrogels and enhance the biological compatibility due to their unique morphology and physicochemical properties.[43] Especially, one-dimensional clay nanotubes have been actively exploited as biological scaffolds component due to their high specific surface area, rigidity, and biocompatibility for boosting mechanical properties of scaffolds and cellular interaction.[44] Thus, one-dimensional clay nanotubes provide promising approaches in biomedical areas as the scaffold materials with the superior mechanical properties and good biocompatibility.

1.4 Clay-based drug carriers

Entrapping of the drug molecules in micro- and nano-particulate systems is a helpful strategy for protecting drugs against chemical and enzymatic degradation, and modulating release into the body. As a result it facilitates aqueous solubility, taste and odor masking, and reduces dissolution rate, and permits site specific delivery.[45]

Over the last decades, clays and biopolymers have been proposed as interesting materials for new drug delivery systems to encapsulate or entrap the drug molecules. A lot of efforts have been devoted to modify polymers by incorporation of inorganic fillers to obtain composites with improved properties.[46] In the last few decades, hybrid systems composed of clay particles dispersed in a polymer matrix have been designed to obtain polymer-clay nanocomposites with new and improved properties which may not be found in the materials composed of each component. One of the problems for the design of drug delivery is the burst release of encapsulated or entrapped drugs. By controlling the release kinetics of drug, therapeutic effects of the drug can be optimized and its biological activity also can be modulated. Silicate based polymer nanocomposites demonstrate good barrier properties due to the tortuous diffusion pathways where drug molecules must travel in order to pass the material. The release rate is controlled by the interaction between the clay and the polymer matrix, which led to an increase in the tortuosity. This property of the nanocomposites can be exploited towards the development of sustained drug release applications.[47,48]

Halloysite and Imogolite clay nanotubes allow the design of smart composite materials with the controlled release of chemically active agents due to their unique surface chemistry and tubular structure. Their inner lumen can store and release molecules in a controllable manner making these nanocontainers attractive for applications in drug delivery and regenerative medicine, self-healing composites, and antimicrobial materials.[49] Controlled release of drug molecules from nanotubes

11

embedded in a polymer matrix provides new long lasting properties to material composites. The release time of drug molecules may be adjusted from tens of hours to months providing sustained functionality.[50] Above all, clay nanotube-based polymeric composites allows the design of smart composite materials with synergistically improved mechanical and rheological properties, and adhesivity combined with controlled release of drug molecules for targeted drug delivery. Thus, it is very perspective for functional tubule biocomposites useful for oral and transdermal drug formulation, skin care, medical implants and dentistry.

1.5 Scope of thesis

This thesis deals with the representative clay nanotubes, i.e. imogolite and halloysite nanotubes as structural nano-fillers for hyaluronic acid hybrid hydrogels. Hyaluronic acid is naturally occurring biopolymer which is used in various biomedical application areas from cell and therapeutic delivery to in vitro scaffolds for creating and controlling the cellular environments. Compared to the other polysaccharides, hyaluronic acid nanocomposite hydrogels exploiting clay nanotubes have not been studied until now because of its unique properties such as high viscosity and extremely sticky and slippery behavior. In this thesis, this study aims to investigate the physiological properties of clay nanotube/hyaluronic acid hybrid hydrogels based on the interfacial interaction of organic-inorganic network architecture. Additionally, curcumin as one component of turmeric, which has powerful antioxidant and anti-inflammatory benefits but poorly absorbed in the body due to its hydrophobic nature, is chosen as a model drug for investigating the efficient curcumin loading into and sustained release from halloysite to fully exploit the advantage of nanotubular structure of halloysite. In chapter 2, finely dispersed imogolite is entrapped in the hyaluronic acid polymer network by crosslinking reaction of EDC chemistry. Preparation mechanism and characterization of imogolite/hyaluronic acid hybrid hydrogels are described. In chapter 3, halloysite surface are modified with silane coupling agent for photo-crosslinking reaction in the hyaluronic acid polymer matrix to overcome the charge repulsion. The optimal mechanical properties are characterized by changing the ratio of modified halloysite. In chapter 4, the release kinetics of curcumin loaded into selectively modified halloysite lumen are described. Finally, concluding remarks are given in chapter 5.

References

[1] F. Bergaya, G. Lagaly (Eds.), Developments in Clay Science Volume 5, Second Edition, Hand Book of Clay Science, Elsevier Ltd., Netherlands, **2013**.

[2] P. Yuan, A. Thill, F. Bergaya (Eds.), Developments in Clay Science Volume 7, *Nanosized Tubular Clay Minerals; Halloysite and Imogolite*, Elsevier Ltd., Netherlands, **2016**.

[3] S. Ijima, *Nature* **1991**, 354, 56.

[4] R. Tenne, *Nat. Nanotechnol.* **2006**, 1, 103.

[5] R. Tenne, R. Rosentsveig, A. Zak, Phys. Status Solidi A **2013**, 210, 2253.

[6] M. Alexandre, P. Dubois, *Mater. Sci. Eng*. **2000**, 28, 1.

[7] M. Ristić, I. Czakó-Nagy, S. Musić, A. Vértes, *J.Mol.Struct*. **2011**, 993, 120.

[8] K. Yamamoto, H. Otsuka, A. Takahara, *Polym. J.* **2007**, 39, 1-15.

[9] W. O. Yah, K. Yamamoto, N. Jiravanichanun, H. Otsuka, A. Takahara, *Materials* **2010**, 3, 1709.

[10] W. Ma, W-O. Yah, H. Otsuka, A. Takahara, *J. Mater. Chem.* **2012,** 22, 11887.

[11] K. Shikinaka, Y. Koizumi, Y. Osada, K. Shigehara*, Polym. Adv. Technol.* **2011**, 22, 1212.

[12] N. Jiravanichanun, K. Yamamoto, K. Kato, J. Kim, S. Horiuchi, W. O. Yah, H. Otsuka, A. Takahara*, Biomacromolecules* **2012**, 13, 276.

[13] N. Teramoto, A. Hayashi, K. Yamanaka, A. Sakiyama, A. Nakano, M. Shibata, *Materials* **2012**, 5, 2573.

[14] K. Ishikawa , T. Akasaka , Y. Nodasaka , N. Ushijima , M. Kaga , S. Abe , M. Uo , Y. Yawaka , M. Suzuki , F. Watari . *Nano Biomedicine* **2009**, 1, 109.

[15] L. Guimarães, A. N. Enyashin, J. Frenzel, T. Heine, H. A. Duarte, G. Seifert, *ACS Nano* **2007**, 1, 362.

[16] Y. Lvov, W. Wang, L. Zhang, R. Fakhrullin, *Adv. Mater.* **2016**, 28, 1227.

[17] M. Massaro, G. Lazzara, S. Milioto, R. Noto, S. Riela, *J. Mater. Chem. B* **2017**, 5, 2867.

[18] W. O. Yah, H. Xu, H. Soejima, W. Ma, Y. Lvov, A. Takahara, *J. Am. Chem. Soc.* **2012**, 134, 12134.

[19] W. O. Yah, A. Takahara, Y. M. Lvov, *J. Am. Chem. Soc.* **2102**, 134, 1853.

[20] J.-C. Gayet, G. Fortier, *J. Controlled Release* **1996**, 38, 177-184.

[21] E. A. Appel, X. J. Loh, S. T. Jones, F. Biedermann, C. A, Dreiss, O. A, Scherman, *J. Am. Chem. Soc.* **2012**, 134, 11767-11773.

[22] N. A. Choudhury, S. Sampath, A. K. Shukla, *Energy Environ. Sci.* **2009**, 2, 55-67.

[23] K. Y. Lee, D. J. Mooney, *Chem. Rev.* **2001**, 101, 1869-1880

[24] G. D. Nicodemus, S. J. Bryant, *Tissue Eng., Part B* **2008**, 14, 149-165.

[25] I. M. El-Sherbiny, M. H. Yacoub, Glob. *Cardiol. Sci. Pract.* **2013**, 38, 316-342.

[26] H. M. Shewan, J. R. Stokes, *J. Food Eng.* **2013**, 119, 781-792.

[27] E. Caló, V. V. Khutiryanskiy, *Eur. Polym. J.* **2015**, 65, 252-267

[28] Y. Zhao, B. Liu, L. Pan, G. Yu, *Energy Environ. Sci.* **2013**, 6, 2856-2870.

[29] A. Razmjou, Q. Liu, G. P. Simon, H. Wang, *Environ. Sci. Technol.* **2013**, 47, 13160-13166.

[30] B. V. Slaughter, S. S. Khurshid, O. Z. Fisher, A. Khademhosseini, N. A. Peppas, *Adv. Mater.* **2009**, 21, 3307-3329.

[31] N. C. Hunt, L. M. Grover, *Biotechnol Lett*. **2010**, 32, 733-742.

[32] N. Annabi, A. Tamayol, J. A. Uquillas, M. Akbari, L. E. Bertassoni, C. Cha, C. U. Gulden, M. R. Dokmeci, N. A. Peppas, *Adv. Mater*. **2014,** 26, 85-124.

[33] T. R. Hoare, D. S, Kohane, *Polymer* **2008,** 49, 1993-2007.

[34] Y. Qiu, K. Park, *Adv. Drug Delivery Rev*. **2012**. 64. 49-60.

[35] A. Vashist, Y. K. Gupta, Sharif Ahmad, *J. Mater. Chem. B* **2014**, 2, 147-166.

[36] N. A. Peppas, J. Z. Hilt, A. Khademhosseini, R. Langer, *Adv. Mater*. **2006,** 18, 1345-1360

[37] P. E. Dietmar, C. Krutzler, F. Keplinger, M. J. Vellekoop, *Lab Chip* **2014,** 14, 378-383.

[38] P. Schexnailder , G. Schmidt, *Colloid Polym Sci*. **2009**, 297, 1.

[39] A. K. Gaharwar, N. A. Peppas, A. Khademhosseini, *Biotechnol. Bioeng.* **2014**, 111, 441.

[40] Peppas NA, Hilt JZ, Khademhosseini A, Langer R,   *Adv. Mater*. **2006**, 18, 1345.

[41] A. R. Hirst , B. Escuder, J. F. Miravet, D. F. Smith, *Angew. Chem. Int.* Ed. **2008**, 47, 8002.

[42] M. A. C. Stuart, W. T. S. Huck, J. Genzer , M. Müller, C. Ober, M. Stamm, G. B. Sukhorukov , I. Szleifer, V. Tsukruk, M. Urban, F. Winnik, S. Zausher, I. Luzinov, S. Minko, *Nat. Mat.* **2010**, 9, 101.

[43] K. Haraguchi, *Polym. J.* **2011**, 43, 223.

[44] E. A. Naumenko, I. D. Guryanov, R. Yendluri, Y. M. Lvov, R. F. Fakhrullin, *Nanoscale* **2016**, 8, 7257.

[45] C. Aguzzi, P. Cerezo, C. Viseras and C. Caramella, *Appl. Clay Sci.* **2007**, 36, 22.

[46] C. Viseras, C. Aguzzi, P. Cerezo, M. C. Bedmar, *Materi. Sci. Technol.* **2008**, 24, 1020

[47] S. Pavlidou, C. D. Papaspyrides, *Prog. Polym. Sci.* **2008**, 33, 1119.

[48] C-J. Wu, A. K. Gaharwar, P. J. Schexnailder, G. Schmidt, *Materials* **2010**, 3, 2986.

[49] Y. Lvov, E. Abdullayev, *Prog. Polym. Sci.* **2013**, 38, 1690.

[50] T. G. Shutava, R. F, Fakhrullin, Y. M. Lvov, *Curr. Opin. Pharmacol.* **2014**, 18, 141.

Chapter 2

Effect of Imogolite Nanotubes as Nano-fillers on Hyaluronic Acid Hybrid Hydrogels

2.1 Introduction

Hydrogels derived from natural polysaccharides are ideal tissue engineering scaffold materials as they resemble the extracellular matrices (ECM) of tissues consisting of various glycosaminoglycans (GAGs).[1] Scaffolds should mimic the structure and biological function of native ECM.[2] Well-known feature of native ECM is the nano-scaled dimensions of their dynamic structure which offers structural and anchoring support to the cells to improve tissue architecture.[3] There are still challenges to design the nanostructured scaffold materials that can match the mechanical properties, tissue-specific structural signals, controlled degradation profile, and cell-scaffold/ECM interaction when they are engineered to the native ECM.[4]

Nanocomposite polymer hydrogels are defined as cross-linked polymer networks swollen with water in the presence of nanoparticles or nanostructures. Nanoparticles play a role in not only crosslinking the hydrogel, adsorbing or attaching to polymer chains, but also adding new properties to the hydrogel by being combined with the polymeric network.[5,6]

Clay nanocomposite hydrogels are very attractive biomaterials for a biotechnology when it comes to designing mechanically strong gels and scaffolds with long-term biocompatibility and controlled biodegradability for tissue engineering.[7,8] Clay nanotubes such as imogolite (IG), which are frequently used in nanocomposite materials as a nano-filler, showed a good cell adhesion and growth in human osteoblast like cells cultivation.[9]. IG is an aluminosilicate nanotubular clay mineral which has a high aspect ratio and specific surface area. It has a unique surface chemistry that outer and inner surfaces are composed of aluminol groups (Al-OH) and silanol groups (Si-OH), respectively. These features make it attractive for utilization in biomedical applications.[10]

Hyaluronic acid (HA) hydrogels are good candidate for articular cartilage repair because they are the component of extracelluar matrix cartilage tissue in human body. HA is a linear polysaccharide that

consists of repeating disaccharide units of D-glucuronic acid and N-acetyl glucosamine linked by glucosidic bonds. They are abundant in articular joint, vitreous humor, and synovial fluid in human body.[11,12] Due to the short half-life of HA in the body, HA should be first stabilized by crosslinking to obtain non-soluble hydrogels with longer residence time and a mechanical strength.[13,14] Hyaluronic acid interacted with biopolymer or clay materials resulted in the composite hydrogels as a scaffold with the good mechanical strength and space for cellular activity.[15,16]

In the current study, freeze dried imogolite is dispersed in neutral HA buffer solution to get a finely dispersed hybrid hydrogels. Imogolite is entrapped in the crosslinked HA network by EDC chemistry.

This study aims to characterize the physicochemical properties of imogolite/hyaluronic acid hybrid hydrogels for potential biomedical applications.

2.2 Experimental

2.2.1 Materials

HA ($M_w = 1.6 \times 10^6$ D) was purchased from Sigma-Aldrich (USA). Tetraethyl orthosilicate (TEOS), acetic acid, hexamethylenediamine (HMDA), 1-ethyl-3-(3-dimethylaminopropyl) carbodiimide hydrochloride (EDC), N-hydroxybenzotriazole (HOBt), 2-morpholinoethanesulfonic acid (MES), bovine testes hyaluronidase were purchased from Tokyo Chemical Industry (Japan). Aluminum chloride hexahydrate ($AlCl_3 \cdot 6H_2O$), sodium hydroxide (NaOH), hydrochloric acid (HCl; 1N), phosphate buffered saline solution (PBS; 0.01M, pH 7.2 – 7.4) were purchased from Wako Pure Chemicals (Japan). All chemicals were used as received without further purification.

2.2.2 Preparation of IG

IG was synthesized according to the methods reported by Farmer et al. Briefly, aqueous solution of tetraethyl orthosilicate $[Si(OEt)_4]$ was stirred for an hour as to be entirely hydrolyzed. After then, Aluminum chloride hexahydrate $[AlCl_3 \cdot 6H_2O]$ was mixed with the above solution. Aqueous sodium hydroxide (0.1 M) was slowly added to the mixture solution until the solution reach the pH 5. Subsequently, the cloudy mixture solution was then reacidified by 1 mmol of hydrochloric acid and 2 mmol of acetic acid and adjusted the solution volume to 1 L with deionized water, resulting in the transparent solution with the concentration of 2.4 mmol L^{-1} with regard to Al and 1.4 mmol L^{-1} for Si.

The solution was then refluxed at 369 K for 4 days. After being cooled to room temperature, saturated NaCl (8.6 mmol L^{-1}) solution was added to the mixture solution. The gelated solution was filtered and rinsed with deionized water thoroughly. The obtained imogolite gel was redispersed in weak acidic solution by sonication. A cotton-like imogolite was finally obtained by freeze-drying the dispersed solution.
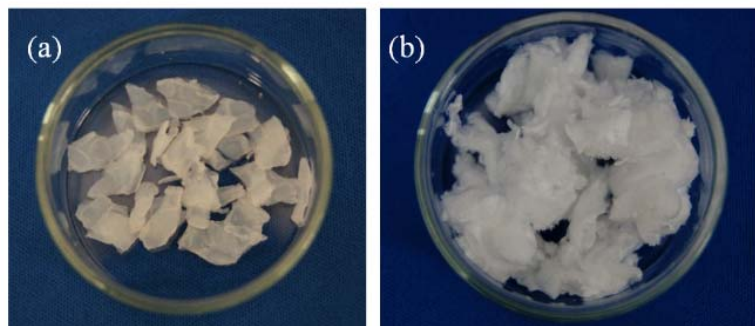
2.2.3 Preparation of hydrogels

2.2.3.1 Preparation of HA-HMDA hydrogels (IG-0)

HA hydrogels were prepared according to a procedure reported by Yeom et al with slight modification.[42] HMDA was dissolved in 0.01 M MES buffer solution (pH 6.7) containing 0.154 M NaCl. HA powder was dissolved in the HMDA solution, and the concentration was adjusted to 2.0 % (w/v). Molar ratio of HMDA to carboxyl groups in HA was 1/1. EDC (4 molar equivalent to HA) and HOBt (2 molar equivalent to HA) were dissolved in deionized water, and added to the HA solution. The solution pH was adjusted to 6.7 by the addition of 1 M HCl, and the solution was stirred vigorously for 10 minutes. The precursor solution was incubated at 310 K for 1 hour to complete the cross-linking reaction. The as-prepared self-standing hydrogels were used as samples for rheology test and compression mechanical test. The self-standing hydrogels (denoted as IG-0) were dialyzed with PBS solution for 24 hours at 310 K in incubator at a rotation speed of 100 rpm to remove the unreacted reagents, and the purified gels were used for swelling test and enzymatic degradation test.

2.2.3.2 Preparation of IG/HA-HMDA hybrid hydrogels (IG-1, IG-5, IG-10)

IG was finely dispersed in MES buffer solution at pH 6.7. MES buffer solution with IG contents of

0.02, 0.1, and 0.2 % (w/v) were prepared. HA was dissolved in the HMDA dissolved MES buffer solution containing IG, and the HA concentration was adjusted to 2.0 % (w/v) to make IG to HA content 1, 5, 10 % (w/w). Subsequent cross-linking was performed by the same procedure as hydrogel preparation described in the above section. Resulting cross-linked hybrid hydrogels were denoted as IG-1, IG-5, IG-10 with respect to IG contents.
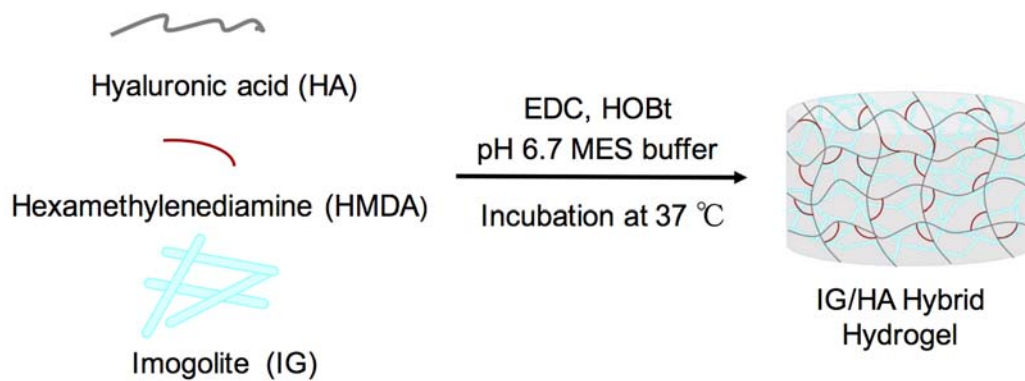
Figure 2-2. Schematic presentation for the preparation of IG/HA hybrid hydrogels.
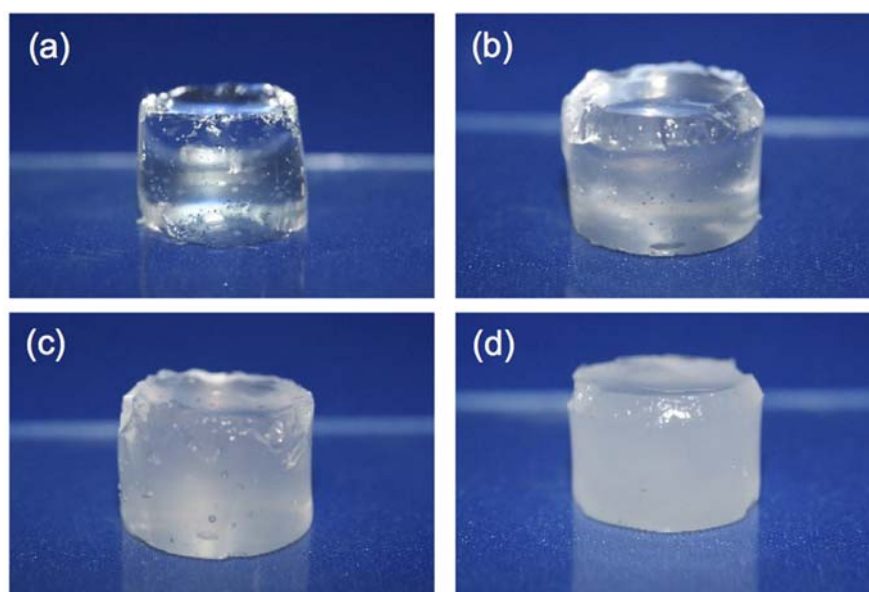
Figure 2-3. Cross-linked native HA hydrogel IG-0 (a), and IG/HA hybrid   hydrogels

IG-1 (b), IG-5 (c), and IG-10 (d)

2.2.4 Characterization of hydrogels

2.2.4.1 Measurements

Fourier transform infrared (FTIR) spectra were measured by Spectrum 100 spectrometer (Perkin Elmer Inc., Waltham, MA, USA) using KBr pellets method. IR spectra were recorded by averaging 64 scans between 4000 and 500 cm^{-1} with the resolution of 4 cm^{-1}. Scanning electron microscopy (SEM) observations were conducted by Real Surface View VE7800 (Keyence Co., Ltd, Osaka, Japan) with applied voltage of 5 kV. The cross-section of hydrogels was obtained by splitting freeze-dried hydrogels immediately after freezing by liquid nitrogen. The cross-sectioned samples were sputter-coated with an osmium layer using HPC-1SW Hollow Cathode Plasma CVD (Shinkuu Device Co., Ltd, Ibaraki, Japan). Compressive mechanical test was carried out by a tensile tester (EZ-Graph, Shimadzu Co., Ltd, Kyoto, Japan) with 50 N load cell at the loading rate of 1 mm/min. The dimension of the samples was cylinder shape with a diameter of 12 mm and a height of 12 mm. Compression tests were performed 6 times for each case of sample at room temperature until the rupture of hydrogels was recorded. The strain was measured from the displacement of the crosshead. Dynamic viscoelasticity was measured by oscillatory rheometer (Physica MCR 101, Anton Paar, Graz, Austria). The dimension of the samples was cylinder shape with a diameter of 16 mm and a height of 2 mm. Parallel plate with a diameter of 20 mm was used and temperature was controlled to 298 K. Amplitude sweep and frequency sweep tests were performed three times for each case of sample.

2.2.4.2 Swelling test

Freeze-dried hydrogels were immersed in PBS buffer solution (0.01 M, pH 7.4), and incubated at 310 K at the rotation speed of 100 rpm to set in vivo environment. Hydrogels were picked up at pre-determined time points and weighed after the removal of excessive surface water. The equilibrium

25

swelling ratio was calculated according to the following equation (1)

Swelling Ratio = $(W_s - W_d)/W_s$ (1)

where W_s and W_d are the weights of the hydrogels in swollen and dry state, respectively.

2.2.4.3 Enzymatic degradation test

Freeze-dried hydrogels were immersed in PBS buffer (pH 7.4) containing hyaluronidase from bovine

testes with the concentration of 4 Unit/ml, and incubated at the rotation speed of 100 rpm at 310 K. At

pre-determined time point, hydrogels were picked up from the enzymatic solution, and washed three

times to remove the salts and enzyme on the surface of hydrogels. The hydrogels were immersed in

ethanol for 2 hours and dried for 1 day at room temperature. The percentage of the weight loss was

calculated according to the equation (2).

Weight Loss (%) = $[(W_i-W_d)/W_i] \times 100$ %   (2)

where W_i is the weight of the initial freeze dried hydrogel and W_d is the weight of the remained dried

hydrogel.

2.3 Results and discussion

2.3.1 Preparation of hybrid hydrogels

IG has an interaction with anionic charged polymers in acidic environment because its isoelectric point is around pH 7. Cross-linking reaction of HA with HMDA is very sensitive to pH because ester intermediate coupling for amide bond formation is generated around neutral pH and the intermediate is necessary to accomplish stable cross-linking reaction of carboxyl groups. Also, buffer solutions without carboxylic groups have to be chosen for stabilization of pH because carboxylic groups in buffer solution are also involved in the carbodiimide-mediated amidation reaction. To balance the stable dispersion and interaction potential of IG with HA and the efficient carbodiimide-mediated cross-linking reaction, pH of the MES buffer solution was adjusted to 6.7. Surface charge of IG is almost neutral at that pH, whereas HA is net negative. Therefore, the hydrophilic IG disperses in the aqueous solution, whereas the electrostatic interaction does not exist in that pH condition, and the neutral charged IG well interacts with negatively charged HA chains by mainly hydrogen bonding and van der Waals interaction. Scheme 1 illustrates the fabrication of the IG/HA hybrid hydrogels through mixing and chemical cross-linking process. A series of hybrid hydrogels with different IG content were prepared, whereas the concentration of HA was unified to 2.0 % (w/v) in this study. The higher amount of IG was incorporated in the hybrid hydrogels, the more turbid hybrid hydrogels were obtained because of the refractive index contrast between the IG aggregates and HA matrix (Figure 1). Because of the absence of electrostatic repulsive interaction of net neutral IG, mutual aggregation of dispersed IG occurs in the large content.

2.3.2 FTIR analysis

Interaction between IG and HA was investigated by FTIR spectroscopy (Figure 2-4). Pristine HA has

a broad OH stretching absorption at 3400 cm^{-1} and a C-H stretching absorption at 2910 cm^{-1}. These

peaks were also shown in all the cross-linked hydrogels. IG shows two OH absorption peaks at 3515

and 1635 cm^{-1} which correspond to the OH stretching and a HOH deformation band due to the tubular

structure of IG. C=O stretching absorption of amide I band and C-N stretching absorption with N-H

bending absorption of amide II band in HA were observed at 1615 cm^{-1} and 1560 cm^{-1}, respectively.

These peaks were shifted to 1620 and 1565 in all the cross-linked hydrogels, and absorption intensity

of the amide II band increased compared with the pristine HA because N-H bending absorption of

amide bonds introduced by cross-linking reaction was overlapped with N-H peak of HA acetamide

groups. OH absorption of IG were not seen in the cross-linked hybrid hydrogels because of the overlap

with OH stretching vibration and amide I band of HA. C-O stretching and N-H bending vibration of

amide III band were observed at 1380 and 1325 cm^{-1} in HA and all the cross-linked hydrogels, but

absorption of N-H bending at 1325 cm^{-1} was increased only in all the cross-linked hydrogels because

of the overlap with N-H absorption introduced by cross-linking reaction. The characteristic absorption

peak of Al-O-Si in IG was observed as two split peak at 990 and 940 cm^{-1}. These characteristic

absorptions shifted to 995 cm^{-1} in hybrid hydrogels. The absorption peaks of C-O-C stretching

vibration at 1040 cm^{-1} in HA and hydrogel without IG (IG-0) were shifted to 1045 cm^{-1} in all the hybrid

hydrogels. These spectroscopic changes indicated that IG does not interrupt the cross-linking reaction

and it interacts with HA chains by hydrogen bonding.
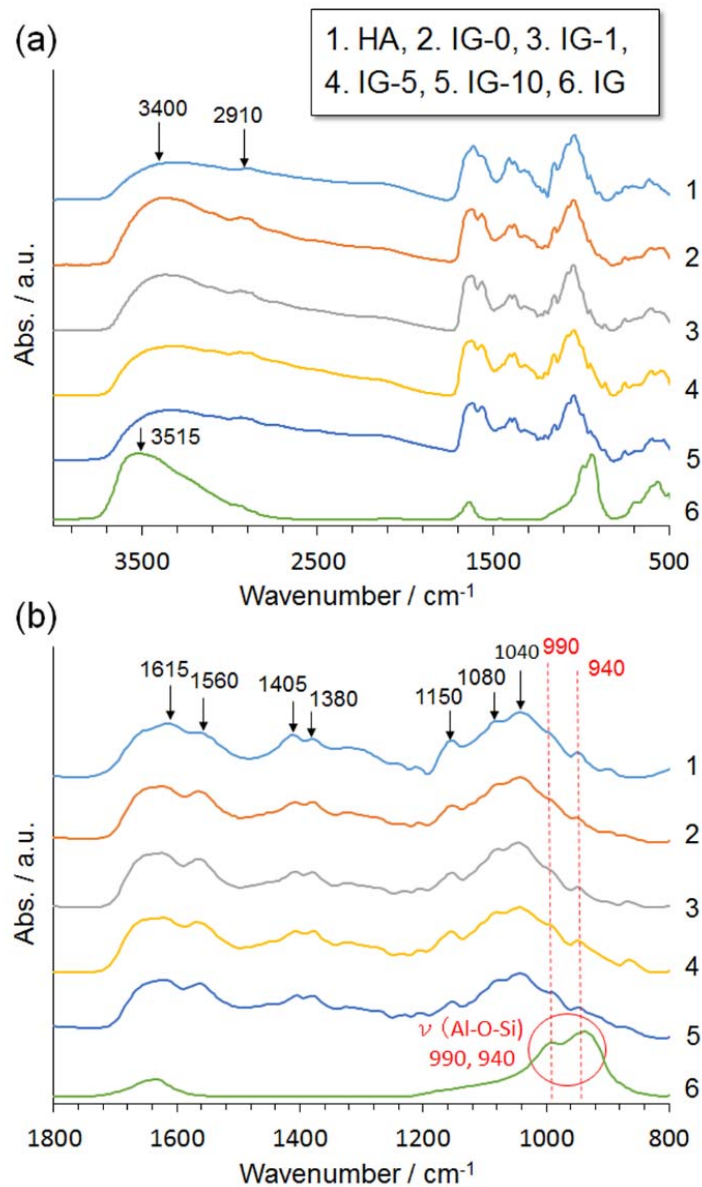
Figure 2-4. FTIR spectra of HA (1), cross-linked hydrogels without IG (IG-0) (2), IG/HA

hybrid hydrogels with a variety of IG content IG-1 (3), IG-5 (4), IG-10 (5), and IG (6) in

the full scale (a) and the region from 800 to 1800 cm^{-1} (b).

2.3.3 Morphology of hybrid hydrogels

SEM cross-section images of the hydrogels were shown in Figure 2-5. HA showed the smallest pore

size and high porosity, but dry HA was easy to rupture without cross-linking reaction. The hybrid

hydrogel with low IG content (IG-1) showed almost similar morphology with the native cross-linked

hydrogel without IG (IG-0), whereas the hybrid hydrogels with high IG content (IG-5 and IG-10)

showed drastically different morphology as compared with the IG-0. The IG-0 and IG-1 represented

homogeneous pore size and interconnected porous network, and the average pore size was over 200

μm. In the case of cross-linked hybrid hydrogels with high IG content, inhomogeneous randomly

collapsed pores with large size distribution were observed. Fibrous aggregates were observed on the

porous wall of IG-5 and IG-10 hybrid hydrogels, indicating that too much IG content induce

aggregation of IG in the HA solution to form IG bundles. This result is well consistent with the opaque

visual of the IG-5 and IG-10 hydrogels. The highly wrinkled transformed porous wall in the hybrid

hydrogels indicates that rigid IG strongly interacts with HA network or each other and it renders the

mechanical strength to the hybrid hydrogels.
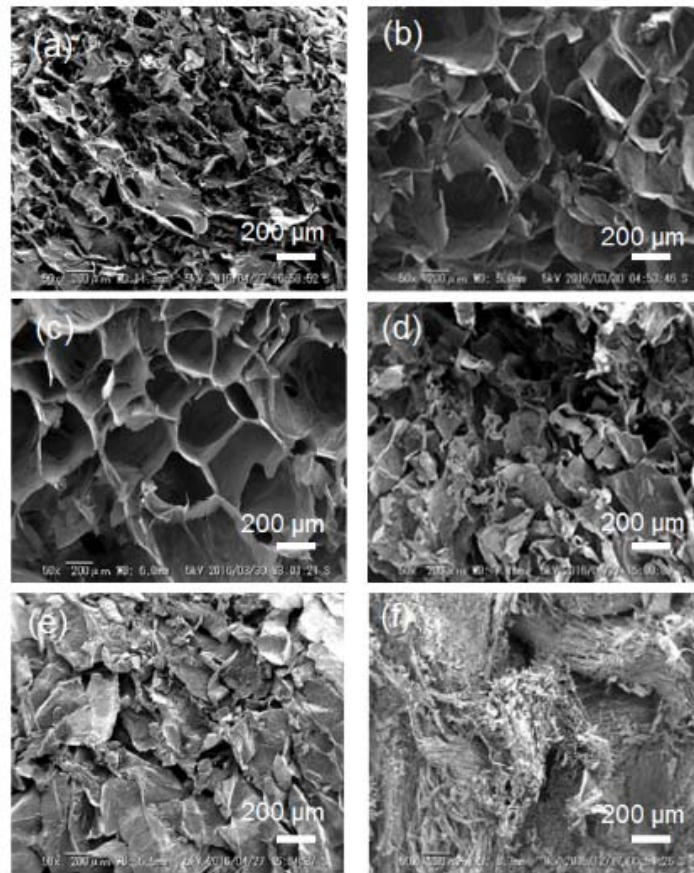
Figure 2-5. SEM cross-section images of HA (a), cross-linked hydrogels IG-0 (b),

IG-1 (c), IG-5 (d), IG-10 (e), and IG (f). Scale bars indicate 200 μm.

31

2.3.4 Swelling properties

Diffusion of nutrients and waste, and cellular migration associate with the swelling ratio and pore size of hydrogel scaffolds. Swelling capability of the hydrogels was measured in the equilibrium swollen state. Time course of swelling ratio of the hydrogels is shown in Figure 2-6. All the hydrogels showed the rapid increase of weight in 2 hours. This relatively rapid swelling continued until 8 hours, and then the water uptake rate became slow and finally reached the equilibrium swollen state within 72 hours from the view point of the weight of swollen hydrogels. IG-0 showed the highest equilibrium swelling ratio whereas IG-10 showed the lowest swelling equilibrium swelling ratio. The more IG contents shows the less swelling ratio, and the order was kept throughout the swelling process. The swelling behavior is well associated with the morphology. The higher porosity and larger pore size hydrogels shows the higher water uptake. Although the IG-10 had the smallest swelling ratio, it still kept 82 % swelling ratio of IG-0. This result indicates that the incorporation of IG into hydrogels still retains the good water uptake capacity due to the hydrophilicity of IG networks.
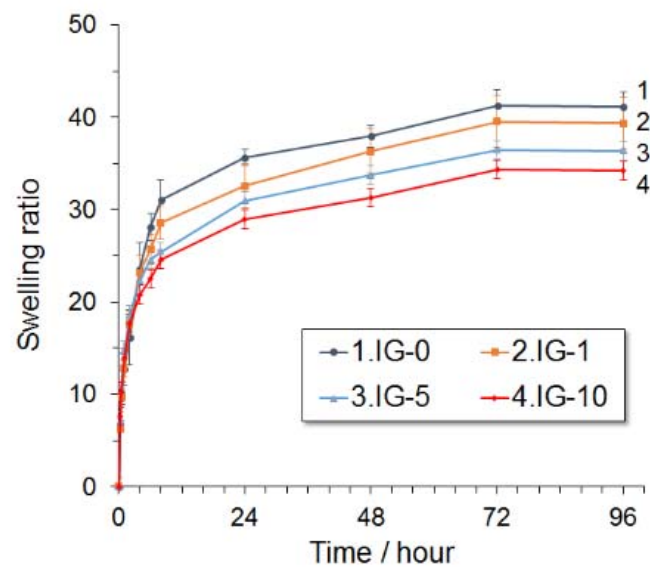
Figure 2-6. Evolution of swelling ratio of native hydrogel IG-0 (1) and IG/HA hybrid hydrogels IG-1

(2), IG-5 (3), and IG-10 (4) in PBS buffer solution with pH 7.4 at 310 K. Error bars represent standard

deviation (n = 3).

2.3.5 Compressive mechanical properties

Mechanical properties of hybrid hydrogels were investigated by compression test (Figure 2-7). Compression strength of the IG-5 hybrid hydrogels was 4 times the IG-0 hydrogels, and the stress at break increased along with the IG contents, indicating that the IG network reinforces the bio-organic charged polymer network. But the IG-10 hybrid hydrogels showed lower strain at break than the IG-5 hybrid hydrogels. The large IG bundle-like aggregates in IG-10 would induce fracture through the generation of voids at the interface of IG aggregates and HA hydrogel matrix.
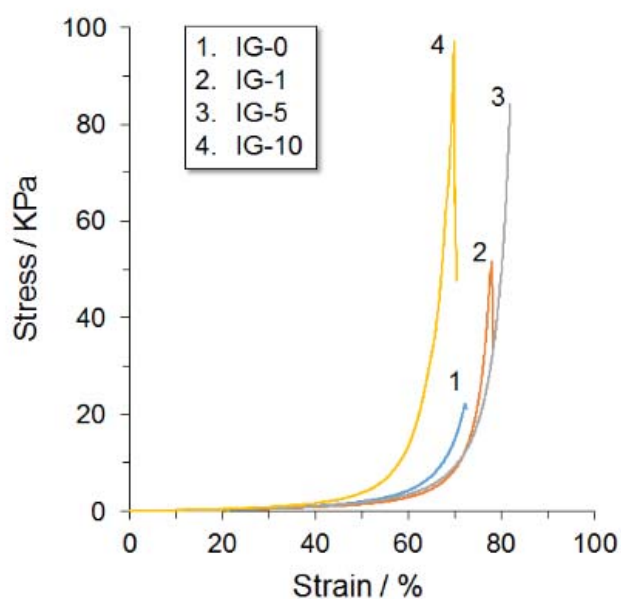
Figure 2-7. Stress-strain curves for native hydrogels IG-0 (1), and IG/HA hybrid hydrogels IG-1 (2), IG-5 (3), and IG-10 (4) (n = 6).

2.3.6 Rheological properties

Frequency sweep test was performed over a physiological frequency range (0.1 – 100 rad/sec) with the fixed strain amplitude of 5 % in the linear viscoelastic region (Figure 6). Storage modulus (G') was higher than the loss modulus (G'') all over the frequency ranges in all the hydrogels, which corresponds to the general gel-like behavior indicating stable self-standing hydrogel with well-developed global network structures. IG-1 showed lower elastic modulus than that of IG-0 in the full frequency ranges. But the values are within the error bound, therefore we can regard that rheological behavior of these two hydrogels are almost the same, indicating that small amount of IG hardly makes a reinforcement of hydrogel network. Whereas IG-10 showed the highest storage modulus which is 3 times the IG-0 because of the additional rigid inorganic network structure. In the case of IG-0 and IG-1 hydrogels, G'' increased along with the frequency. That is regarded as typical fluid-like behavior, so that the high frequency impact energy dissipates as thermal motion. On the other hand, IG 5 and IG 10 hydrogels showed higher G'' values at lower frequency which is a typical viscoelastic behavior of high concentration clay suspension. The drastic increase of G'' in IG 5 and IG 10 hydrogels indicate that IG builds inorganic network structure in the organic polymer network. Because the chemical cross-linking of HA and HMDA was conducted in the presence of well dispersed IG network, so-called interpenetrating hybrid polymer network structure was constructed. Rigid inorganic network was built up via cross-section of well-dispersed fibrous inorganic rigid nanotube. The IG interacted with chemically cross-linked HA/HMDA network to stabilize the network structure as shown in the rheological behavior in Figure 2-8. But the inorganic network was separated momentarily from the organic polymer network at higher stress resulting in the fluid-like behavior of a single organic polymer network.
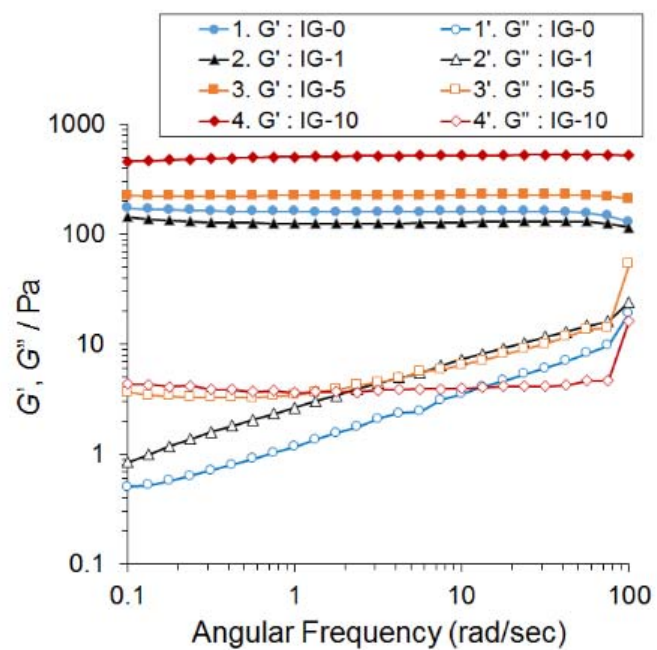
Figure 2-8. Frequency sweep test of native hydrogels (IG-0) (1) and IG/HA hybrid hydrogels IG-1

(2), IG-5 (3), IG-10 (4) in the fixed strain amplitude of 5 % at 25 ℃ (n = 3).

2.3.7 Enzymatic degradation

Hydrogels are normally used as scaffolds for tissue regeneration and they should be either degraded or adsorbed to the body after injection or implantation. Whereas hydrogels need to keep the mechanical strength over a certain period of time to maintain the shapes during the fulfillment of sufficient cell function or wound healing against the cell culture or enzyme activity. Figure 2-9 shows the in vitro enzymatic degradation behavior of hydrogels designating the percentage of weight loss according to the incubation time. The IG-0 and IG-1 hydrogels degraded rapidly in the first 6 hours, and degraded entirely within 48 hours due to the weak mechanical strength as seen in the compressive and the rheological properties. IG-5 and IG-10 hybrid hydrogels showed a significant delay in the initial degradation stage, and the degradation rate is obviously slower than that of the IG-0 and IG-1. The IG-5 and IG-10 remained about 20% after 24 hours, whereas the IG-0 and IG-1 almost completed the degradation at the same time period. After 48 hours, the IG-5 and IG-10 remained ca. 3.8 % and ca. 8.5 % of their initial weight, respectively. The inorganic network of IG significantly prevents the progress of the enzymatic degradation. The hyaluronidase is net negative in physiological condition (pH 7.4 buffer solution) because the isoelectric point ranges from 5 to 6. The outer surface of IG has weak positive charge around pH 7.4. Therefore, the IG network would interact with the hyaluronidase by electrostatic interaction, and the enzymatic activity would reduce. The steric hindrance of the IG network would disturb the diffusion of enzyme into the HA matrix to lead to the contact frequency reduction. The delay in the degradation rate is attributed to the synergetic effect of the reduction in enzymatic activity and contact frequency.
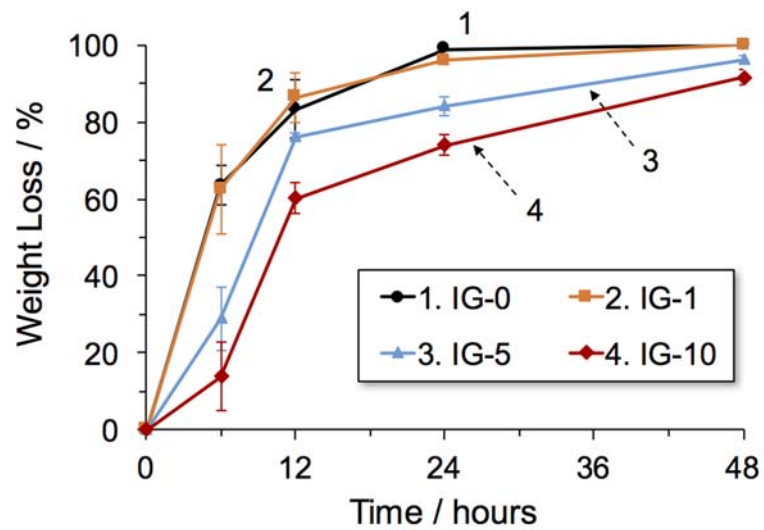
Figure 2-9. Time course of weight loss of native hydrogels (IG-0) (1) and IG/HA hybrid hydrogels IG-1 (2), IG-5 (3), IG-10 (4) in PBS buffer solution of pH 7.4 containing 4 U/ml hyaluronidase in a shaking incubation with 100 rpm at 310 K (n = 3).

2.4 Conclusion

In this chapter, hybrid hydrogels were prepared at neutral pH condition to balance the stable reaction and dispersion of IG in the HA polymer matrix. IG was finely dispersed without significant aggregation. IG reinforced the hydrogel matrix via interfacial interaction between HA chains and inorganic rigid network structure based on the result of compression and rheology test. Higher amount of IG affected the increment of shear modulus and fracture strain up to 5 wt % which indicate the optimal mechanical properties. The gap of fracture stress between IG-5 and IG-10 was not so much big. IG/HA hybrid hydrogels retains the good swelling capacity as much as native hydrogels due to the hydrophilicity of IG network which is an essential factor in regenerative scaffold application. Hybrid hydrogels with higher IG content showed the slower degradation rate because of the steric hindrance of inorganic network and electrostatic interaction of surface charge leading to lower contact frequency to HA network and the reduction of enzymatic activity. Overall, optimal formulation of IG can affect the performance of HA hybrid hydrogels that is highly requested in biomedical applications.

References

[1] J. Zhu, R. E. Marchant, *Expert Rev. Med. Devices* **2011**, 8, 607.

[2] F. J. O'Brien, *Mater. Today,* **2011**, 14, 88.

[3] H. Geckil, F. Xu, X. Zhang, S-J. Moon, U. Demirci, *Nanomedicine* **2010**, 5, 469.

[4] R. J. Wade, J. A. Burdick, *Mater. Today*, **2012**, 15, 454.

[5] P. Schexnailder, G. Schmidt, *Colloid Polym Sci*. **2009**, 287, 1.

[6] A. K. Gaharwar, N. A. Peppas, A. Khademhosseini, *Biotechnol. Bioeng*. **201**4, 111, 441.

[7] C-W, Chang, A. Spreeuwel, C. Zhang, S. Varghese, *Soft Matter*, **2010**, 6, 5157.

[8] C. Aimé, T. Coradin, J. *Polym. Sci., Part B: Polym. Phys*. **2012**, 50, 669.

[9] K. Ishikawa, T. Akasaka, S. Abe, Y. Yawaka, M. Suzuki, F. Watari, *Bioceram. Dev. Appl.* **2011**, 1, 1.

[10] W. Ma, W. O. Yah, H. Otsuka, A. Takahara, *J. Mater. Chem.* **2012**, 22, 11887

[11] G. Kogan, L. Soltés, R. Stern, P. Gemeiner, *Biotechnol. Lett*. **2007**, 29, 17-25.

[12] J. A. Burdick, G. D. Prestwich, *Adv. Mater*., **2011**, 23, H41.

[13] P. Bulpitt, D. Aeschlimann, *J. Biomed. Mater. Res*., **1999**, 47, 152-169.

[14] S-K. Hahn, J-K. Park, T. Tomimatsu, T. Shimoboji, *Int. J. Biol. Macromol.*, **2007**, 40, 374-380.

[15] M. D. Brigham, A. Bick, E. Lo, A. Bendali, J. A. Burdick, A. Khademhosseini, *Tissue Eng., Part A* **2009**, 15, 1645.

[16] D. Bhatnagar, D. Xu, D. Gersappe, M. H. Rafailovich, *J. Chem. Biol. Interfaces* **2014**, 2, 1.

[17] V. C. Farmer, A. R. Fraser, J. M. Tait, *J. Chem. Soc. Chem. Commun.,* **1977**, 462.

[18] J-S. Yeom, S-H. Bhang, B-S. Kim, M-S. Seo, E-J. Hwang, I-H. Cho, J-K Park, S-K. Hahn, *Bioconjugate Chem.* **2010**, 21, 240.

Chapter 3

Hybrid Hydrogels Based on Halloysite Nanotubes and Hyaluronic Acid

3.1 Introduction

In this chapter, halloysite nanotubes (HNTs), another analogous to imogolite nanotube, was applied to preparation of hyaluronic acid hybrid hydrogels. The outer surface of HNTs is composed of silanol groups (Si-O-Si), while the inner surface is aluminol groups (Al-OH). Contrary to the structure of imogolite, the inner surface of HNTs is positively charged to capture the negatively charged molecules in the lumen, whereas the outer surface is negatively charged to interact with the positively charged molecules.

HA-based hydrogels encapsulating functional nanoparticles are promising candidate for artificial extracellular matrix for cellular growth and regeneration in tissue-engineered constructs. However, its weak mechanical properties restrict the range of applications.[2]

HA/HNTs hybrid hydrogels with improved mechanical properties were suggested in the current study. HA was modified with 2-aminoethylmethacrylate (AEMA) for photo-crosslinking reaction which can facilitate the encapsulation of functionalized nanoparticles or biomolecules.[3-4] HNTs were also modified with a silane coupling reagent which has an acrylate group.[5-7] Hybrid hydrogels were prepared by photo-crosslinking reaction exploiting acrylate groups of modified HA and HNTs. This study investigated how the modified HNTs affect the physicochemical properties in HA polymer networks compared to pristine HNTs.

3.2 Experimental

3.2.1 Materials

HA (M_w = 1.6 $\times 10^6$ Da) and 2-aminoethylmethacrylate hydrochloride (AEMA), Irgacure 2959 (2-hydroxy-4β-(2-hydroxyethoxy)-2-methyl-propiophenone) were purchased from Sigma-Aldrich (USA). 3-acryloxypropyltrimethoxysilane (APTMS), hydroquinone, 2-morpholinoethanesulfonic acid (MES) and 1-ethyl-3-(3-dimethylaminopropyl) carbodiimide hydrochloride (EDC) was purchased from Tokyo Chemical Industry (Japan). N-hydroxysuccinimide (NHS), sodium hydroxide (NaOH), hydrochloric acid (HCl; 1N), and phosphate buffered saline solution (PBS; 0.01M, pH 7.2–7.4) were purchased from Wako Pure Chemical (Japan).

3.2.2 Modification method of HA-AEMA

Carboxylate group of HA repeat unit was conjugated by amide bond as reported previously. Briefly, HA 0.3 g was dissolved in MES buffer solution (0.1% w/v, pH 6.5) including 50 mM MES and 0.5 M NaCl. Subsequently, NHS 4.6 mmol and EDC 9.2 mmol were added to the solution. After 5 min, AEMA 4.6 mmol was added to the solution and the mixture was stirred for 24 h. HA modified with AEMA (HA-AEMA) solution was dialyzed for 3 days in deionized water using dialysis bag (MWCO 6-8 kD), filtered, and freeze-dried.

3.2.3 Modification method of mHNTs

The surface of HNTs was modified with 3-acryloxypropyltimethoxysilane coupling agent. The surface of HNTs was activated by stirring HNTs in 2N HCl for 2 h before silanization. Dried HNTs (1.0 g) were dispersed in dry toluene (40 mL) which contained hydroquinone (0.001 g) as an inhibitor. 3-Acryloxypropyltrimethoxysilane (APTMS, 2.0 mL) was dissolved in dry toluene (40 mL), and the APTMS solution was introduced to the HNTs dispersion. The suspension was refluxed at 80 °C under

stirring for 20 h. HNTs powder modified with APTMS (denoted as mHNTs) was purified by washing with toluene and ethanol/water (30:70) mixed solvent. mHNTs were filtered and dried overnight at 110 °C under vacuum.

3.2.4 Photo-crosslinking reaction of hybrid hydrogels

HA-AEMA with and without mHNTs. The freeze-dried HA-AEMA was dissolved in a mixed solvent (ethanol/water:30/70) including mHNTs and 0.05% (w/v) Irgacure 2959. HA-AEMA concentration was adjusted to 2.0% (w/v). The mHNTs ratio to HA-AEMA was adjusted to 0%, 2.5%, 5%, 10%, and 20% (w/w). Photo-crosslinking reaction was triggered by 365 nm UV light irradiation for 5 min at the intensity of 1 mW/cm^2. The photo-crosslinked hydrogels with the different mHNTs content were designated as HA-mHNTs 0, 2.5, 5, 10, and 20, respectively. Hybrid hydrogels with 10% (w/w) pristine HNTs (HA-HNTs 10) were also prepared as a control sample through the same preparation process.
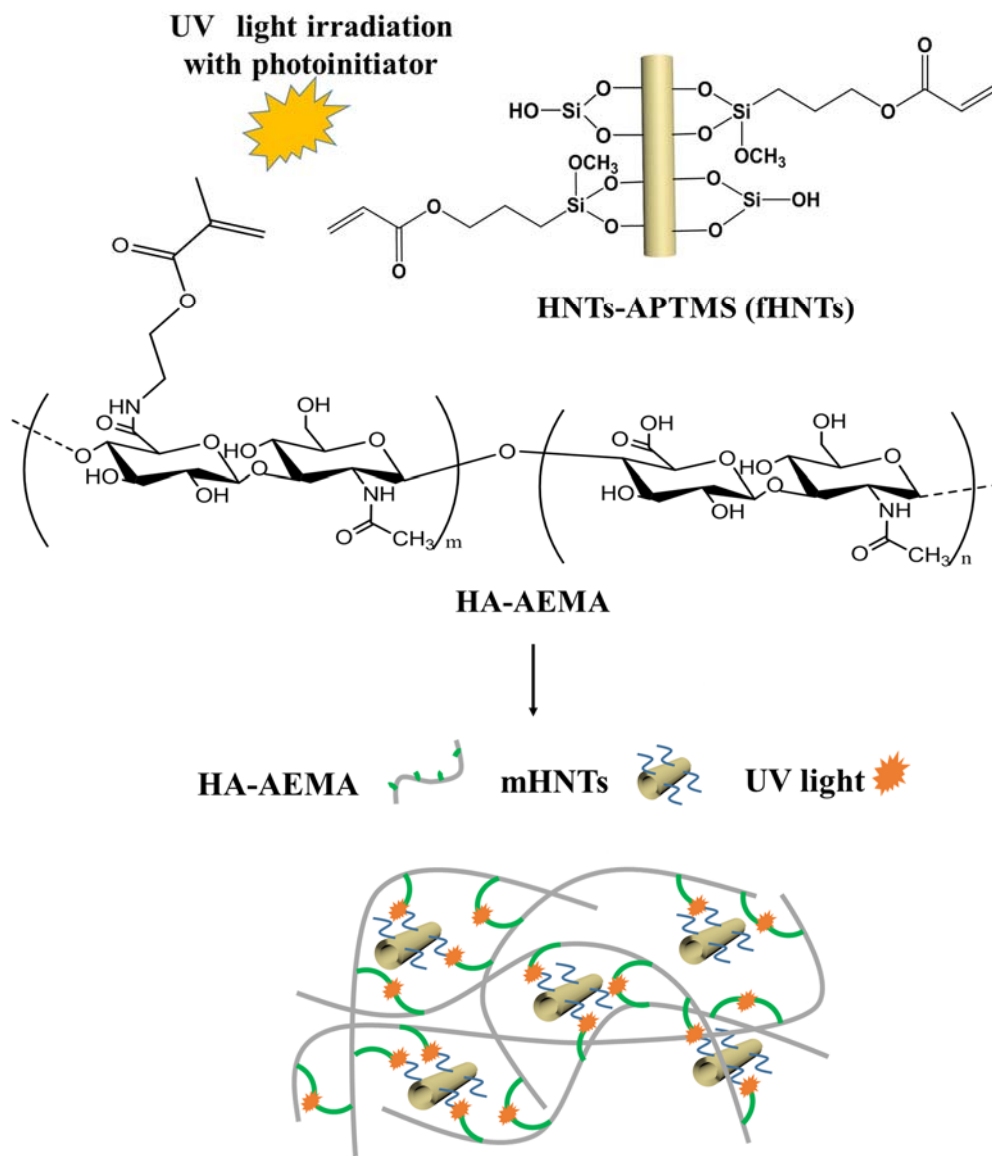
Figure 3-1. Schematic representation of the photo-crosslinking reaction of HA-mHNTs hybrid hydrogels.
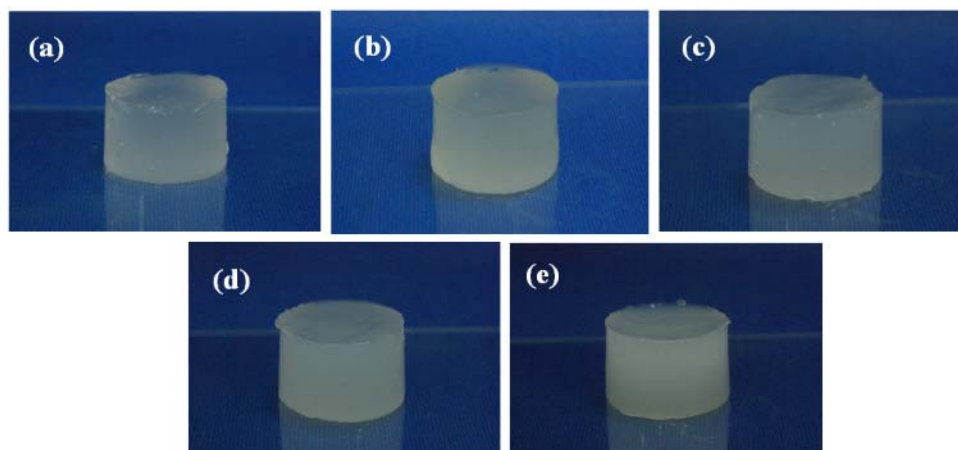
Figure 3-2. Photo of photo-crosslinked hydrogels : IG-0 (a), IG-1 (b), IG-5 (c), IG-10 (d), IG-20 (e).

3.2.5 Characterization

3.2.5.1 ^{1}H NMR spectra

The degree of substitution (DS) of methacrylate group in HA-AEMA was determined by ^{1}H NMR spectroscopy with a 400 MHz BRUKER spectrometer (Bruker Biospin GmbH, Rheinstetten, Germany).

3.2.5.2 Wide angle X-ray diffraction measurement

. The Wide angle X-ray diffraction (WAXD) patterns of HNTs and mHNTs were obtained by X-ray diffractometer SmartLab (Rigaku, Osaka, Japan) using Cu Kα (λ= 0.154 nm) radiation.

3.2.5.3 FTIR measurement

Fourier transform infrared (FTIR) measurement was carried out by Spectrum 100 Spectrometer (Perkin Elmer Inc., Waltham, MA, USA) with a resolution of 2 cm^{-1} at room temperature. IR data were

collected using 64 scans in the range of 4000 – 450 cm^{-1} with KBr powder method.

3.2.5.4 Rheology

Dynamic oscillatory shear tests were performed by Physica MCR 101 (Anton Paar, Graz, Austria). Linear viscoelastic region was previously determined by amplitude sweep test at 1 Hz. The temperature was set to 298 K and gap between the upper plate and the sample was 1 mm. The sample was fully swollen in PBS buffer solution (pH 7.4). Parallel plate with a diameter of 20 mm was used for amplitude and frequency sweep test.

3.2.5.5 Compression test

Compression tests were performed by EZ-Graph (Shimadzu Co., Ltd, Kyoto, Japan). Hydrogels for compression test were fully swollen in PBS buffer solution (pH 7.4) before measurement. 50 N load cell was used at the loading rate of 1 mm/min. The dimension of the samples was cylinder shape with a diameter of 10 mm and a height of 10 mm.

3.2.5.6 Swelling test

For swelling test, freeze-dried hydrogels were immersed in PBS buffer solution (0.01 M, pH 7.4), and incubated at 310 K at the rotation speed of 100 rpm. Equilibrium swelling ratio was determined as follows : $(W_s - W_d)/W_s$, (W_s : the weight of fully swollen hydrogel, W_d : the weight of fully dry hydrogel)

3.3 Results and discussion

3.3.1 HA modification by AEMA

Degree of substitution (DS) of methacrylate group in HA-AEMA was calculated from the integral

ratio of b and c. DS was approximately 40%.
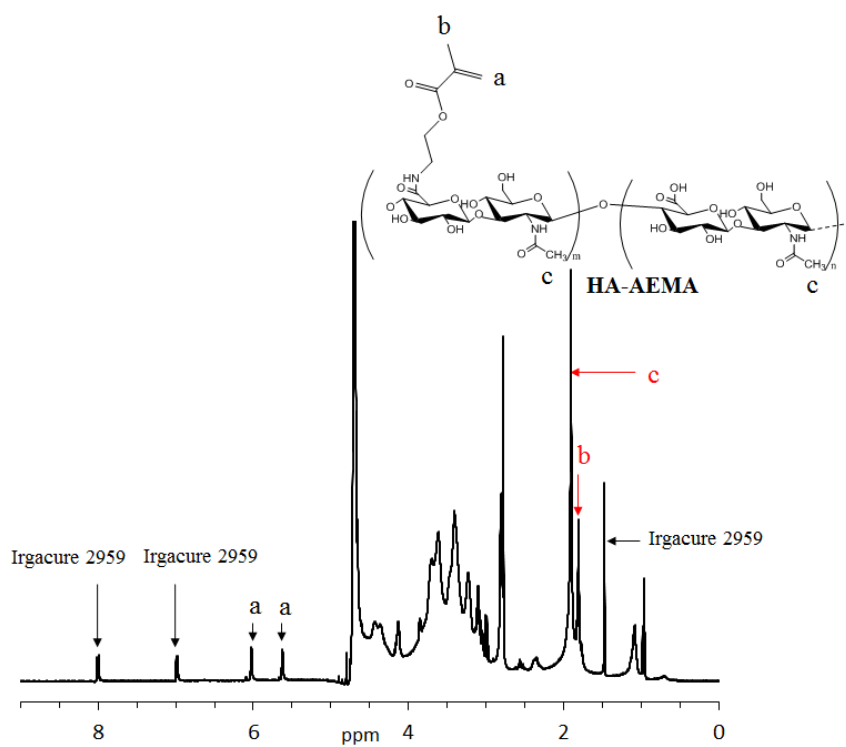
Figure 3-3. ^{1}H NMR spectrum of HA-AEMA

3.3.2 Wide-angle X-ray diffraction profiles

The tubular structure of mHNTs was verified to be identical to the activated dried HNTs and pristine HNTs based on wide-angle X-ray diffraction measurement. mHNTs maintained 0.72 nm wall-packing spacing.
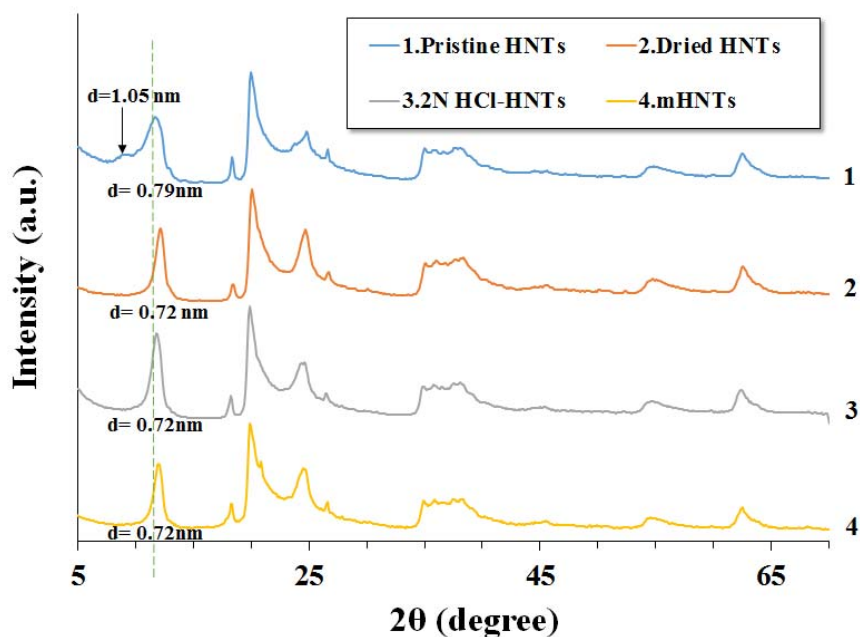
Figure 3-4. Wide-angle X-ray diffraction profiles of pristine HNTs (1), dried pristine HNTs (2), HNTs activated by soaking in 2N HCl (3), and mHNTs (4).

3.3.3 FTIR analysis

FTIR spectra demonstrated that HNTs were successfully modified with 3-acryloxypropyltrimethoxysilane (APTMS), and confirmed the formation of hybrid hydrogels (Figure 3.5). mHNTs had absorptions at 2950 cm^{-1}, 1710 cm^{-1}, 1385 cm^{-1}, and 1315 cm^{-1} assigned to the stretching vibration of CH$_2$ and C=O, and deformation vibration of CH$_2$ and Si-CH of APTMS, respectively. The HOH bending vibration band was observed at 1625 cm^{-1} due to the tubular structure

of HNTs. The absorption of the stretching vibration of C=C bond in the acrylate groups around 1620 cm^{-1} was overlapped with the absorption of HOH bending vibration of adsorbed water in HNTs interlayer (Figure 3-5; 8 and 9). A shoulder peak at 1705 cm^{-1} is assigned to C=O stretching vibration of the amide bond in HA-AEMA. The absorption peak at 3695 and 3615 cm^{-1} are ascribed to the stretching vibration of inner-surface and inner hydroxyl groups of Al-OH, respectively.[8-10] These characteristic peaks were strongly observed in the high content mHNTs hybrid hydrogels (HA-mHNTs 10 and HA-mHNTs 20). The in-plane Si-O stretching vibration at 1015 cm^{-1}, and O-H deformation vibration of inner hydroxyl groups of Al-OH at 910 cm^{-1} were not clearly observed in the hybrid hydrogels due to the overlap of C-O-C and C-C stretching vibration of HA.
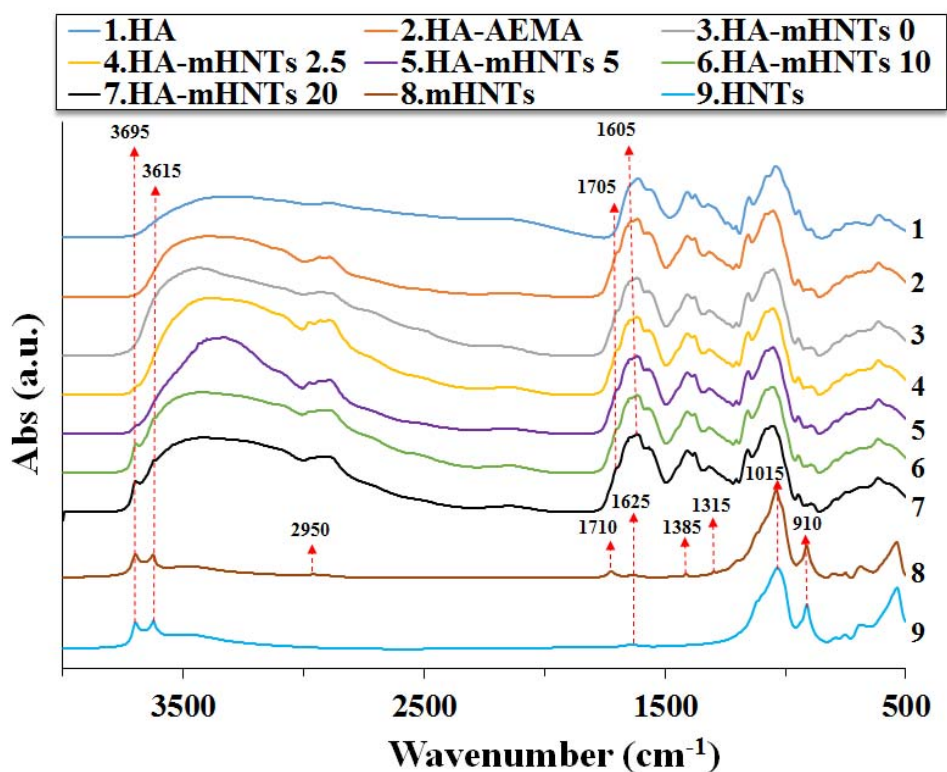
Figure 3-5. FTIR spectra of HA (1), HA-AEMA (2), a native hydrogel without mHNTs (HA-mHNTs 0) (3), hybrid hydrogels with a different content of mHNTs: HA-mHNTs 2.5 (4), HA-mHNTs 5 (5), HA-mHNTs 10 (6), HA-mHNTs 20 (7), mHNTs (8), and pristine HNTs (9).

3.3.4 Rheological properties

Dynamic oscillatory shear test revealed the mechanical properties of the viscoelastic hybrid hydrogels as a function of frequency after photo-crosslinking reaction. Viscoelastic properties were evaluated in the frequency range of 0.1-10 Hz at 298 K. All the hydrogels showed higher storage modulus (G′) than loss modulus (G″) in a whole frequency region and relatively plateau G′ values indicating a typical elastic gel. Especially, G′ values of HA-mHNTs 10 were predominantly larger than those of the other hydrogels indicating the highest stiffness and effective reinforcement of the hybrid hydrogel by mHNTs (Figure 3-6a-4). All the hydrogels except HA-mHNTs 10 showed a frequency-dependent gradual increase in G′ values from 5 Hz indicating the stiffening of HA entanglement network (shear thickening). Interestingly, G″ values in the hybrid hydrogels increased along with the mHNTs content up to 10%, suggesting effective energy dissipation in the network reinforced by mHNTs. G′ of HA-HNTs 10 (Figure 3-6a-6) and HA-mHNTs 20 (Figure 3-6a-5) showed a similar trend but much lower values. G″ of HA-HNTs 10 (Figure 3-6b-6) showed a significant frequency-dependence. The observed softening in the HA-mHNTs 20 and HA-HNTs 10 is attributed to the low crosslink density due to the aggregation of nanotubes. The incorporation of excessive amount of nanotubes in HA-mHNTs 20 disturbed the dispersion and interaction of the nanotubes with the polymer matrix resulting in the reduced storage and loss moduli. In the case of HA-HNTs 10, the electronegative repulsion between unmodified HNTs surface and HA carboxylate groups may have hindered the dispersion of the nanotubes leading to the aggregation and poor interaction with the polymer matrix.[11]
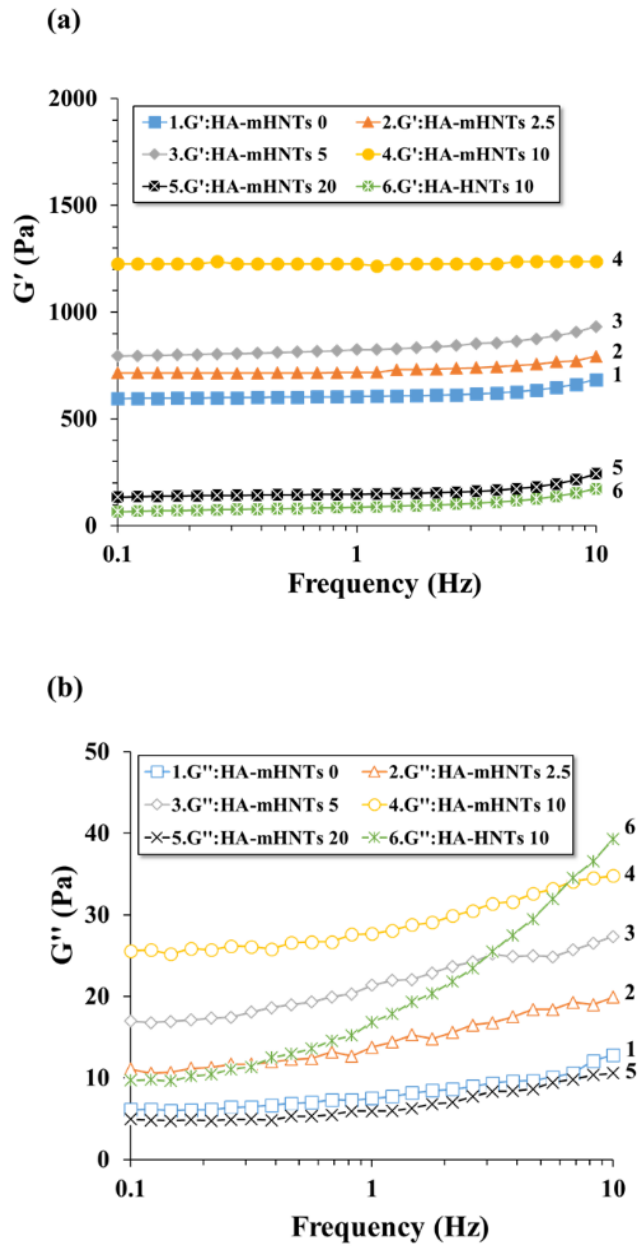
Figure 3-6. Frequency dependence of viscoelasticity of hydrogels: (a) Storage modulus (G′) and (b) Loss modulus (G″) as a function of frequency for HA-mHNTs 0 (1), HA-mHNTs 2.5 (2), HA-mHNTs 5 (3), HA-mHNTs 10 (4), HA-mHNTs 20 (5), and HA-HNTs 10 (6). Strain amplitude was set to 1% within the linear viscoelastic region at 298 K (n=3).

3.3.5. Compressive mechanical properties

Compressive mechanical properties of the hybrid hydrogels were evaluated by uniaxial compression test (Figure 3-7). All the hydrogels showed a non-linear elastic behavior attributed to the typical strain stiffening of the polysaccharide-based hydrogels. The fracture stress increased with the increment of the mHNTs content up to 10%. HA-mHNTs 10 showed a significant increase of compressive stress with the similar fracture strain, indicating the best mechanical performance attributed to the structure integrity and the strong interaction between organic and inorganic networks. On the contrary, HA-mHNTs 20 showed a lower compressive strength than HA-mHNTs 0. In the case of HA-HNTs 10, they exhibited an adverse effect of nano-filler on the mechanical strength resulting in a very brittle hybrid hydrogel. The electronegative repulsion between HA and HNTs promotes the separation and HNTs aggregation. In other words, excessive content of mHNTs and pristine HNTs induce their aggregation in the polymer matrix. We attribute this result to the inhomogeneous organic-inorganic network structure.
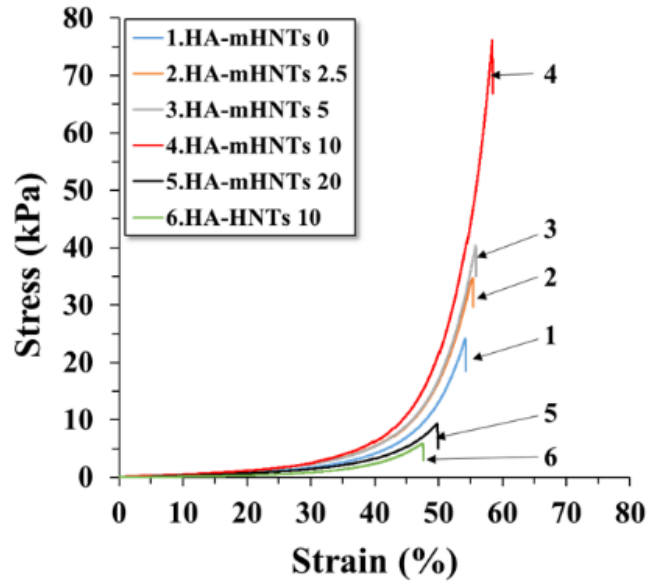
Figure 3-7. Compression test of hybrid hydrogels at 298 K with the compression rate of 1mm/min: HA-mHNTs 0 (1), HA-mHNTs 2.5 (2), HA-mHNTs 5 (3), HA-mHNTs 10 (4), HA-mHNTs 20 (5), and HA-HNTs 10 (6) (n=3)

3.3.6 Swelling behavior

Figure 3-8 shows the time course of swelling ratio of hybrid hydrogels. All the hydrogels reached the equilibrium swelling state within 3 days and showed a relatively similar swelling kinetic and pattern. HA-mHNTs 0 showed the highest equilibrium swelling ratio attributed to the low crosslink density of the organic polymer chains, while the hybrid hydrogels showed the reduction of the water uptake capacity in proportion to the mHNTs content. This trend suggests that the crosslink density was increased by the introduction of the mHNTs. The well dispersed inorganic nanotubes can limit the polymer chain mobility by covalent bonding resulting in the reduction of water absorption ability. In addition, hard nanotube phase is impermeable to the water molecules, which resists the water uptake. However, the reason for the lower swelling ratio of HA-mHNTs 20 can be explained that higher amount of inorganic nanotubes causes the lower diffusion and permeability of water molecules and thus the highest resistance to swelling. In contrast, HA-HNTs 10 may have the predominance of desorption of water molecules over the sorption because of the increase in mobility of the most loosely crosslinked polymer chains resulting in the decrement of the swelling ratio.
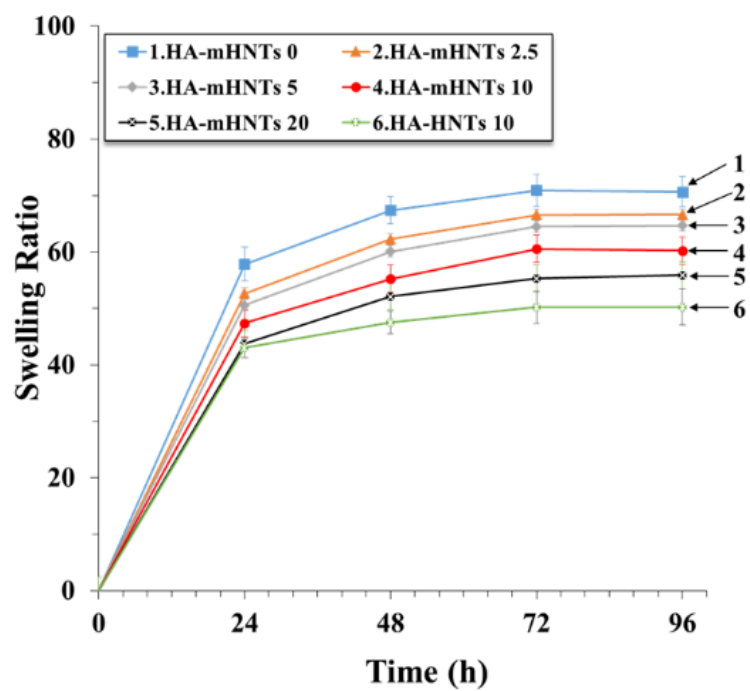
Figure 3-8. Equilibrium swelling ratio of hybrid hydrogels in PBS solution at 310 K: HA-mHNTs 0 (1), HA-mHNTs 2.5 (2), HA-mHNTs 5 (3), HA-mHNTs 10 (4), HA-mHNTs 20 (5), HA-HNTs 10 (6) (n=3).

3.3.7 Morphology of hybrid hydrogels

SEM observation elucidates morphology of the hybrid hydrogels (Figure 3-9). Native crosslinked hydrogels exhibit the regular pore structure with regular pore size (Figure 3-9a). HA-mHNTs 2.5 hybrid hydrogels retain similar pore structure to native hydrogels (Figure 3-9b). The pore structure of HA-mHNTs 5 started to change into the thicker and collapsed pore structure with smaller size in part. HA-mHNTs 10 hybrid hydrogels show drastic change in the morphology. The pore of HA-mHNTs 10 was almost clogged and collapsed, and the vicinity of pore became thicker and the smallest but it still maintained the shape of honeycomb like pore structure elucidating the strong interaction between the HA network and mHNTs by covalent bonding. HA-mHNTs 20 hybrid hydrogels exhibit irregular morphology that consists of big and small pore because of the aggregation of mHNTs in the polymer matrix resulting in hydrogels with weaker mechanical strength than HA-mHNTs 10 despite the high inorganic contents. HA-HNTs 10 hybrid hydrogels showed the largest pore size irregularly resulting in hydrogels with the weakest mechanical strength. The large pore size is associated with the weak mechanical strength of the hydrogels.[12,13] HA-HNTs 10 hybrid hydrogels have the repulsive interaction with HA polymer chain leading to the poor crosslinking density. Thus, they formed the inhomogeneous interconnectivity and larger pore size in the crosslinked polymer matrix randomly.
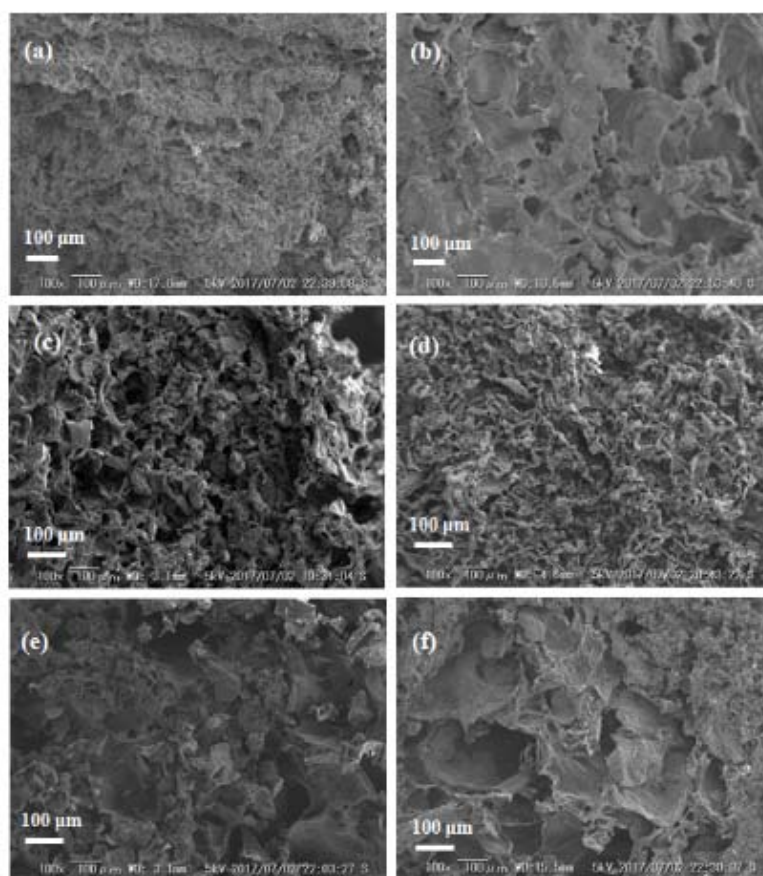
Figure 3-9. SEM images of cross section of HA-mHNTs 0 (a), HA-mHNTs 2.5 (b), HA-mHNTs 5 (c), HA-mHNTs 10 (d), HA-mHNTs 20 (e), and HA-HNT 10 (f) hybrid hydrogels.

3.4. Conclusion

The surface modification of HNTs provided the good mechanical strength and increased fracture strain to the hybrid hydrogels. However, excessive amount of incorporation of HNTs make the hydrogel brittle and easily broken at the lower strain. Pristine HNTs hardly improve the mechanical properties of hybrid hydrogels because of the strong repulsive interaction between negatively charged-HNTs and -HA. Repulsive interaction predominates the hydrogen bonding between hydroxyl group of HNTs and carboxylate group and hydroxyl group of HA. Covalent bonding derived from acrylate groups makes the polymer chains strongly immobilized on the surface of HNTs resulting in the enhanced mechanical strength and better viscoelastic properties. Optimal formulation of mHNTs in the hybrid hydrogels boosted the mechanical properties still retaining good swelling capability that are the prominent factors for scaffolds in biomedical application. SEM photos of microstructure pore reveals that optimally formulate hybrid hydrogels showed the smaller pore size with the ordered interconnectivity because of higher crosslink density between HNTs and HA.

In this study, mHNTs surface functions as a crosslinking point to bond strongly with the polymer matrix resulting in the increased crosslinking density in the polymer matrix.

References

[1] N. G. Veerabadran, D. Mongayt, V. Torchilin, R. R. Price, Y. M. Lvov, *Macromol. Rapid Commun*. **2009**, 30, 99.

[2] M. Liu, X Zeng, C. Ma, H. Yi, Z. Ali,, X. Mou , S. Li, Y. Deng, and N. He, *Bone Res.* **2017**, 5,17014.

[3] O. Jeon, K. H. Bouhadir, J. M. Mansour, E. Alsberg, *Biomaterials* **2009**, 30, 2724.

[4] M. S. Bae, D. H. Yang, J. B. Lee, D. N. Heo, Y. Kwon, I. C. Youn, K. Choi, J. H. Hong, G. T. Kim, Y. S. Choi, E. H. Hwang, I. K. Kwon, *Biomaterials* **2011**, 32, 8161.

[5] H. Jo, F. D. Blum, *Langmuir* **1999**, 15, 2444.

[6] F. Chen, X. Xie, Y. Shi, *Talanta* **2013**, 115, 482.

[7] X. Zhu, H. Li, H. Zhou, S. Zhong, *RSC Adv*. **2015**, 5, 66147.

[8] M. Liu, Y. Zhang, J. Li, C. Zhou, *Int. J. Biol. Macromol*. **2013**, 58, 23.

[9] M. Liu, L. Dai, H. Sji, S. Xiong, C. Zhou, Mater. *Sci. Eng. C* **2015**, 49, 700.

[10] R. T. Silva, P. Pasbakhsh, K. L. Goh, S-P. Chai, H. Ismail, *Polym. Test* **2013**, 32, 265.

[11] S. D. Buffa, E. Grifoni, F. Ridi, P. Baglioni, *J. Nanopart. Res*. **2015**, 17, 146.

[12] S. Lin-Gibson, J. A. Cooper, F. A. Landis, M. T. Cicerone, *Biomacromolecules* **2007**, 8, 1511-1518.

[13] Z. Izadifar, X. Chen, W. Kulyk, *J. Func. Biomater*. **2012**, 3, 799-838.

Chapter 4

Drug Nanocarriers Based on pH Sensitive Halloysite

Nanotubes

4.1 Introduction

Nanocarrier platforms for the controlled delivery of substances have been extensively studied for a couple of decades as they have shown promising results in the area of active anticorrosion,[1,2] drug delivery,[3,4] biosensor,[5] and gas storage.[6] There are several types of nanocarrier such as polymer containers, layered double hydroxides, mesoporous inorganic materials, and halloysite clay nanotubes (HNTs).[7-9] Among them, HNTs can be a prospective candidate as a nanocarrier for the targeted drug delivery and controlled release of biologically active molecules, and chemically active agents.[10] As mentioned in previous chapters, HNTs are regarded as a nanoscale container for the encapsulation and controlled release of drugs due to their unique tubular structure and interesting features such as large aspect ratio, rich functionality, good biocompatibility, and high mechanical strength. Especially, selectively modified HNTs can load the hydrophobic active molecules efficiently into the lumen and they can perform the controlled release.[11,12]

Curcumin, the principal curcuminoid of turmeric, is widely used as spice, food coloring agent and traditional medicine. It has been extensively studied as an anti-oxidant, anti-bacterial, anti-inflammatory, and anti-tumor material for a couple of decades.[13-14] However, curcumin has limitations in clinical applications on account of hydrophobicity, poor absorption, less bioavailability, and rapid metabolism. These problems can be solved by the encapsulation into nanoparticles, liposomes, micelles, and phospholipid complexes which improve the circulation period.[15-16] Curcumin exists in the keto form in the acidic and neutral condition, and in the enol form in the basic condition.[17] The two C=C bonds between 1,3-dicarbonyl and 3-methoxy, 4-hydroxyphenyl parts on each side are important sites for pharmaceutical activities of curcumin.[18]
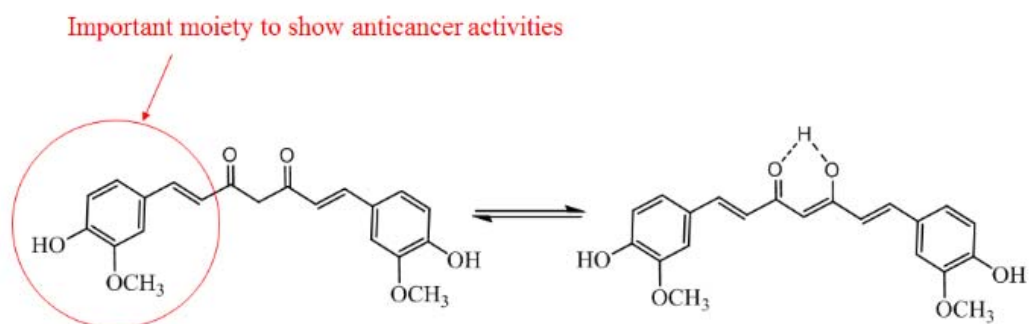
Scheme 1. Keto-enol tautomerism of curcumin

In this chapter, HNTs was studied as a curcumin nanocarrier with stimulus responsive property for controlled release. Dopamine groups was bound to curcumin by Schiff base reaction. The dopamine chemisorbed to inner lumen of HNTs has the reversible interaction according to the pH condition. Curcumin attached to this inner lumen of HNTs was released in controlled and sustained manner compared to the pristine HNTs.

4.2 Experimental

4.2.1 Materials

HNTs were purchased from Sigma-Aldrich (Mo, USA) and used after acid treatment for surface activation. Dopamine hydrochloride and curcumin (synthetic), trimethylamine were purchased from Tokyo Chemical Industry (Tokyo, Japan) and used without further purification.

4.2.2 Preparation of dopamine-curcumin Schiff base (DC)

Curcumin (0.135 mmol; 50 mg) was dissolved in 20 ml of methanol. Dopamine hydrochloride (1.05 mmol; 200 mg) was dissolved in 10 ml of methanol. The dopamine hydrochloride solution was added to the curcumin solution dropwise and refluxed at 50 ℃ with the addition of equivalent molar amount of trimethylamine to dopamine for 6 hr under constant stirring. The mixture solution was cooled to room temperature and evacuated. The collected solid was washed with deionized water thoroughly, filtered, and vacuum dried at 50 ℃.

4.2.3 Dopamine-Curcumin Schiff base loading into HNTs (HNTs-DC)

The dried DC 50 mg was dissolved in 20 ml of methanol. Purified HNTs 500 mg was introduced into the DC solution and stirred for 1 hr. Subsequently, the HNTs suspension was evacuated three times and kept stirring for vacuum state for 1 hr. After evacuation, the suspension was stirred for 24 hr. After stirring, the suspension was centrifuged at 8000 rpm, and the precipitate was washed with deionized water two times and filtered. Supernatant and filtered water was collected to calculate the drug encapsulation efficiency and loading efficiency.

- Encapsulation efficiency (EE, wt %) = $[(C_t - C_s)/C_t] \times 100$ (1)

Where C_t is the total weight of curcumin and C_s is the weight of curcumin in the supernatant.

- Loading efficiency (LE, wt %) = $(C_l/C_h) \times 100$ (2)

Where C_l is the weight of loaded curcumin in HNTs and C_h is the total weight of used HNTs.

4.2.4 Curcumin loading into HNTs (HNTs-C)

Curcumin 50 mg was dissolved in 20 ml of methanol. Purified HNTs 500 mg was introduced into the curcumin solution. Curcumin was loaded into the HNTs with the same method as DC loading. After stirring for 24 hr, the suspension was centrifuged at 8000 rpm, and washed with deionized water two times and filtered. Supernatant and filtered water was collected to calculate the drug encapsulation efficiency and loading efficiency.

4.2.5 HNTs-DC loading into hyaluronic acid (HA-HNTs)

HNTs-DC 1mg was dispersed in 5 ml of deionized water containing HA-AEMA (2% w/v) and Irgacure 2959 (0.05 % w/v) (chapter 3). Photo-crosslinking reaction was triggered by 365 nm UV light irradiation for 5 min at the intensity of 1 mW/cm^2. The loading amount was determined according to the HNTs-DC loading efficiency for release comparison.

4.2.6 Curcumin loading into hyaluronic acid (HA-C)

As a control, pristine curcumin 0.1 mg loaded photo-crosslinked hydrogels were also prepared.

4.2.7 Drug release

DC and curcumin release from HNTs was performed by the dialysis bag diffusion method in the mixture of PBS and ethanol (pH 7.4 and 5.0, 50% v/v). Curcumin 0.1 mg loaded HNTs were dispersed in 2 ml PBS/ethanol mixture and the suspension was introduced into a dialysis bag. Dialysis bag was soaked in 50 ml release medium and incubated at 37 ℃ with a rotation of 100 rpm. As a control, free curcumin 0.1 mg in dialysis bag was also prepared as a control. At regular time intervals, 1 ml of the external release medium was taken and supplemented with the same amount of fresh medium. The release test was conducted at different pH conditions, pH 7.4 and 5.0. The concentration of released

curcumin was measured by UV-vis spectrometer at 430 nm, using 1 ml of pure medium as a blank. The cumulative amount of drug release was calculated in the course of dialysis time as follows

- Drug release (%) = $C_s / C_l \times 100$ (3)

Where C_s is the sum of released curcumin weight and C_l is the weight of curcumin loaded into HNTs. C_l was calculated from LE of HNTs.

4.2.8 Characterization

4.2.8.1 UV-vis spectroscopy measurement

The drug encapsulation and loading efficiency was determined by UV-vis spectrometer (Shimadzu UV-3600). A calibration curve ($R^2 > 0.999$) of curcumin finely dissolved in release medium was determined at 430 nm using a pure release medium as a blank.

4.2.8.2 Thermogravimetric analysis (TGA)

TGA was conducted on a SII-EXSTAR 6000 TG/DTA 6200 in temperature range of 30 to 600 ℃ under 200 mL min^{-1} of N_2 flow rate.

4.2.8.3 Fourier Transform Infrared spectroscopic measurement (FTIR)

Fourier Transform Infrared spectroscopy (FTIR) was recorded by Spectrum One (Perkin-Elmer Japan Co., Ltd) with a resolution of 2 cm^{-1} at room temperature. FTIR data was collected by averaging 64 scans between 4000 and 450 cm^{-1}. The sample disc was prepared by KBr powder method

4.3 Results and discussion

4.3.1 Schiff base reaction between dopamine and curcumin

The C=O of curcumin enol group has the capability to form the imine group (C=N) with the primary amines by Schiff base reaction. This reaction is very versatile to form a different various substituents, which make it attractive in coordination chemistry.[19] This reaction was performed by the addition of equivalent molar amount of triethylamine to dopamine and subsequently the new imine group was formed between dopamine and curcumin. Schiff base reaction is reversible to be hydrolyzed again into ketone and amine group, respectively according to pH. At acidic pH, imine bond is dissociated into ketone and amine forms.[20] Figure 4-1 shows the schematic illustration for Schiff base reaction between dopamine and curcumin and the Schiff base compound entrapment into inner lumen of HNTs. Dopamine catechol group has the high affinity to the metal or aluminum surface and it strongly interacts with the halloysite lumen.[21] Schiff base reaction between dopamine and curcumin was observed by FTIR spectroscopy (Figure 4-2). HNTs show the typical absorption peaks at 3695 and 3620 assigned to O-H stretching of inner surface hydroxyl groups and O-H stretching of inner hydroxyl groups. The peaks at 1025 and 910 cm^{-1} correspond to O-H stretching of in-plane Si-O stretching and O-H deformation of inner hydroxyl groups. After Schiff base reaction, C=O intensity of DC at 1625 cm^{-1} became smaller and new C=N peak at 1580 cm^{-1} appeared. The band of aromatic C=C appeared around 1500 cm^{-1} in both of dopamine and curcumin.
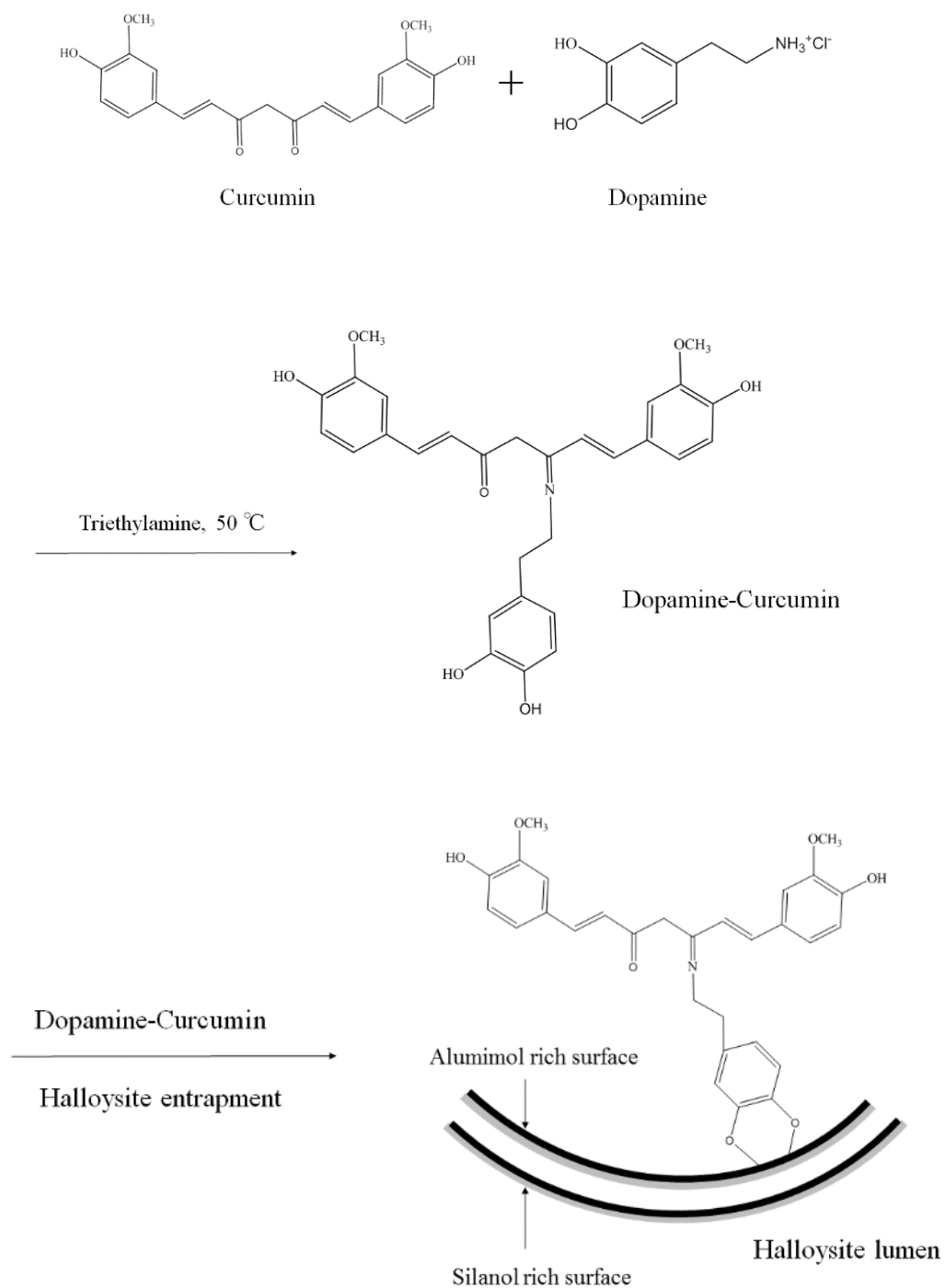
Figure 4-1. Schematic illustration of Schiff base reaction and drug loading into the Halloysite lumen
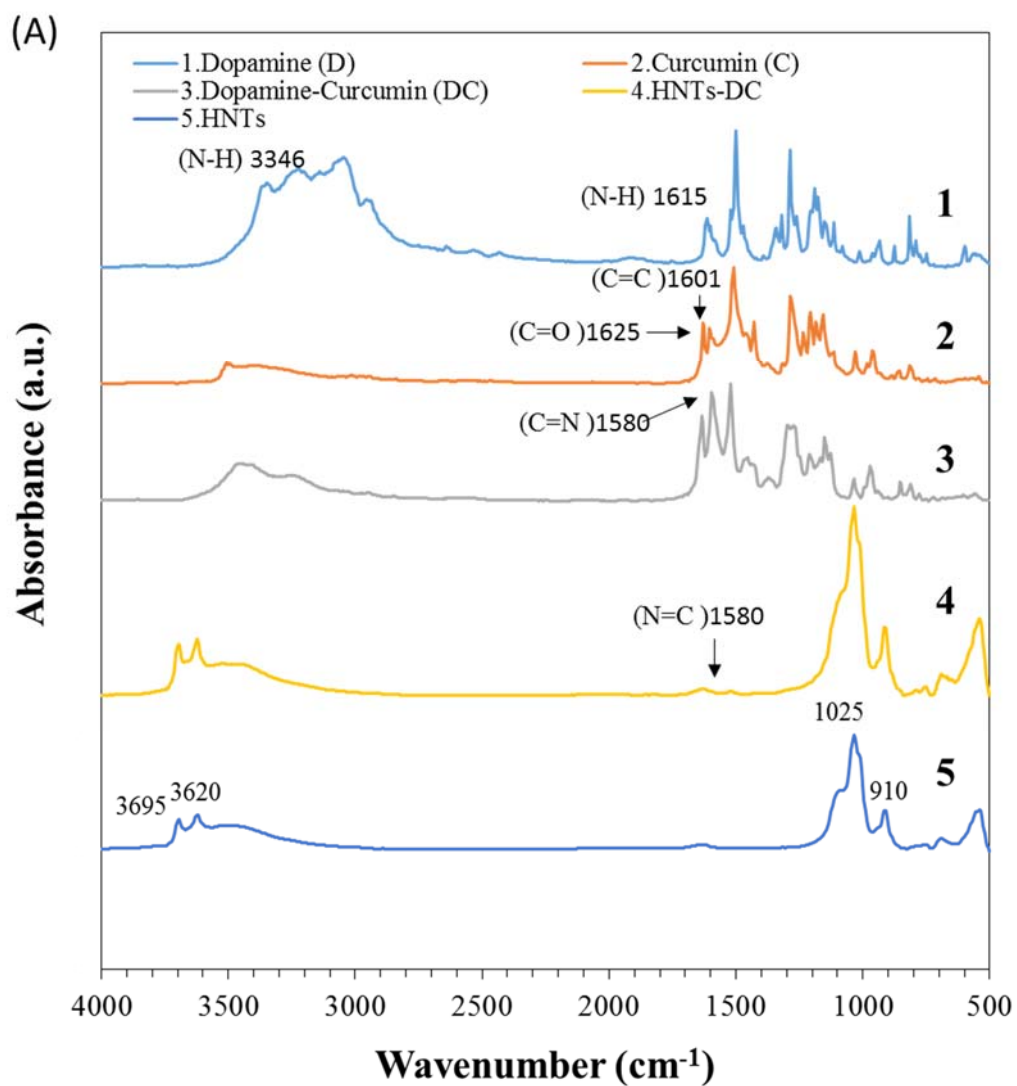
Figure 4-2-A. FTIR spectra of dopamine (1), curcumin (2), DC (3), HNTs-DC (4), HNTs (5) in the full scale region.

(B)
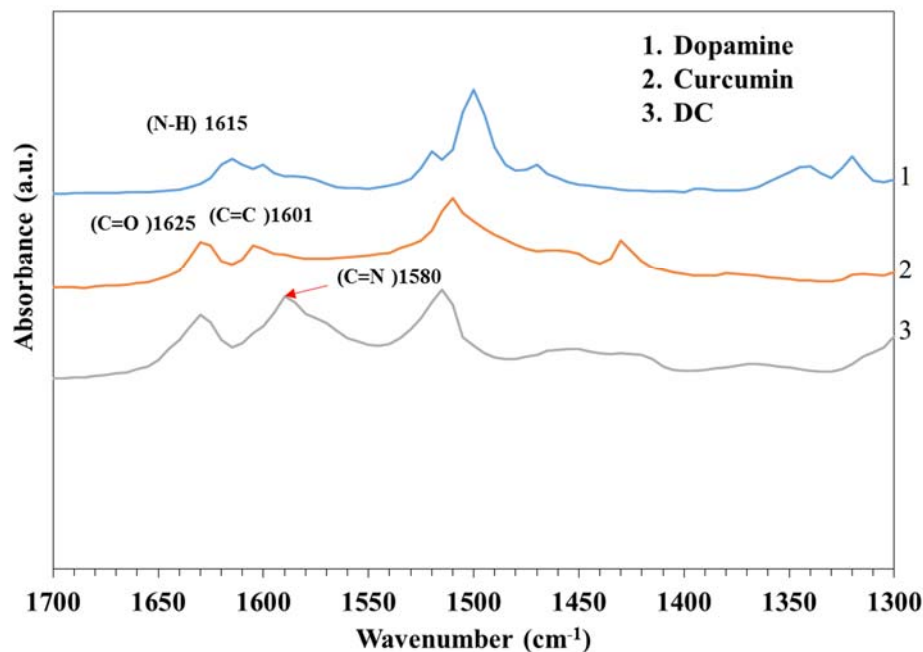
Figure 4-2-B. FTIR spectra of dopamine (1), curcumin (2), Dopamine-Curcumin (DC) (3), HNTs-DC (4), HNTs (5) in the range of 1300 and 2000 cm^{-1}.

Another evidence for formation of Schiff base reaction and dopamine binding to aluminol group was displayed in Figure 4.3. When aluminum plate was immersed in methanol including DC, the solution color changed into brown after 1 week at 37 ℃ incubation. But DC methanol solution including Si wafer did not change the color. The color of curcumin dissolved in methanol including Al plate and Si wafer did not change. This indicates that DC combined with Al by dopamine. When the catechol group of dopamine is oxidized, the color of dopamine solution change into dark brown. The catechol groups adsorb onto the surface of the metals via chemisorption-type interaction.[22,23] XPS spectra in Figure 4.4 also show the strong interaction of dopamine and DC onto Al surface compared to Si wafer. Dopamine chemisorbed Al plate showed the decreased intensity of Al2p compared to the bare Al plate

71

but the dopamine was not found in Si plate, which indicates that dopamine has selective interaction to

Al. Moreover DC still attached to after rinsing the Al plate surface. Surface chemical composition of

the samples are shown in Table 4-1.
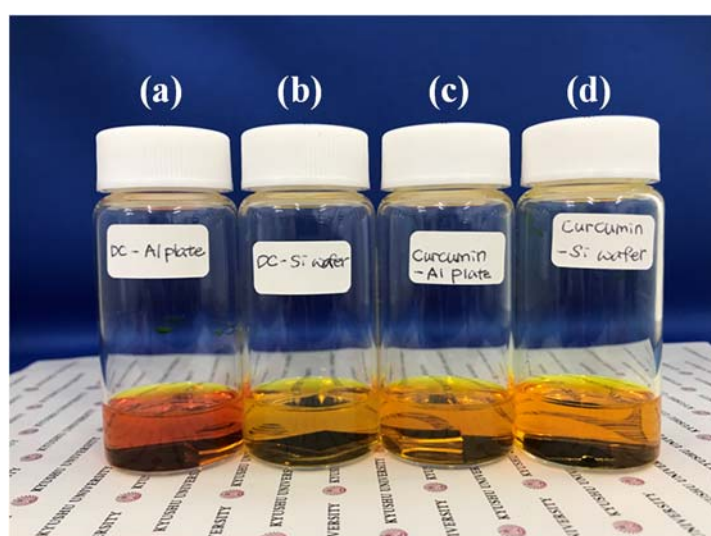
Figure 4-3. Photos of dopamine-curcumin-Al (a), dopamine-curcumin-Si (b), curcumin-Al (c), and

curcumin-Si (4) after incubation at 37 ℃ for 1 week in the dark.

Table 4-1. Atomic percent concentration (%) of Al and Si substrate after treatment of dopamine and dopamine-curcumin

Atomic %	O1s	Al2p	Si2p	C1s	N1s
Substrate					
Al plate	65.7	22.1	-	12.1	<0.1
Si wafer	51.9	-	39.6	8.4	<0.1
Rinse+Sonication					
dopa+Al	47.6	16.3	-	34.9	1.2
dopa+Si	52.7	-	36.1	11.1	<0.1
DC+Al	57.3	17.7	-	24	0.9
DC+Si	51.9	-	36.6	11.5	-
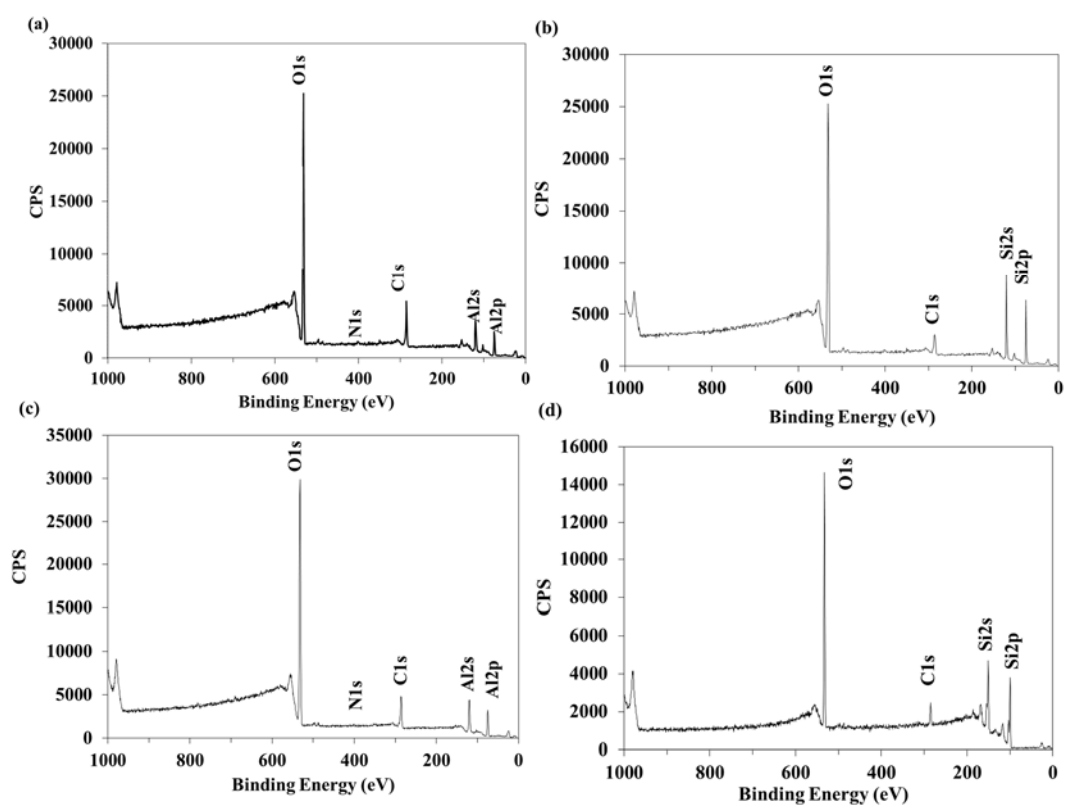
Figure 4.4. XPS spectra of dopa-Al (1), dopa-Si (2), DC-Al (3), DC-Si (4).

4.3.2 Stability of dopamine-curcumin Schiff base

Curcumin has a peak at 430 nm and a shoulder at 360 nm. The peak at 430 nm is attributed to the enol group while the peak at 360 nm was attributed to the keto group of curcumin.[24] Figure 4.5 shows the UV-vis spectra of curcumin and DC to indicate the stability of curcumin after Schiff base reaction. They did not degraded after Schiff base reaction and dry process at 50 ℃.
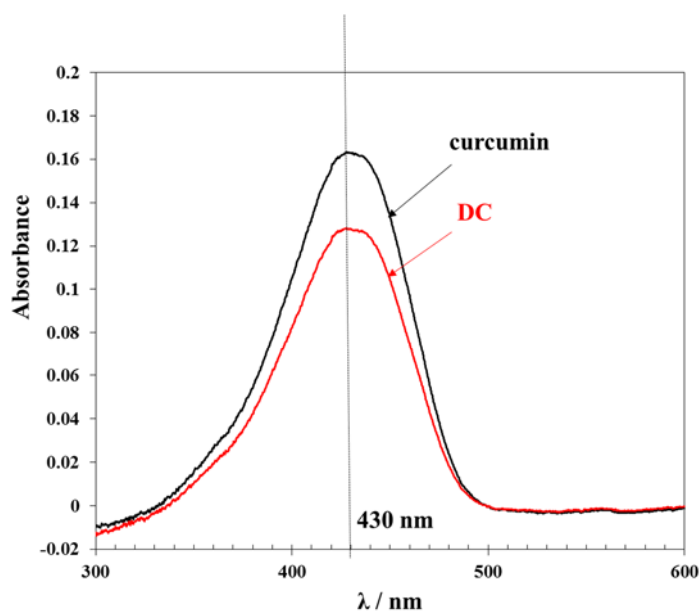
Figure 4.5. Absorbance spectra of curcumin and DC in ethanol

4.3.3 Curcumin loading efficiency

The encapsulation efficiency of HNTs-DC was 85.23 % and loading efficiency was 4.26 %. In the case of HNTs-C, encapsulation efficiency was 92.52 % and 4.62 %, respectively. There was almost no difference in loading weight. However, the weight difference measured by TG between pristine HNTs and HNTs-C was 2.24 %. The gap of loading amount compared to UV-vis determination might be attributed to the error of collecting supernatant after rinsing.
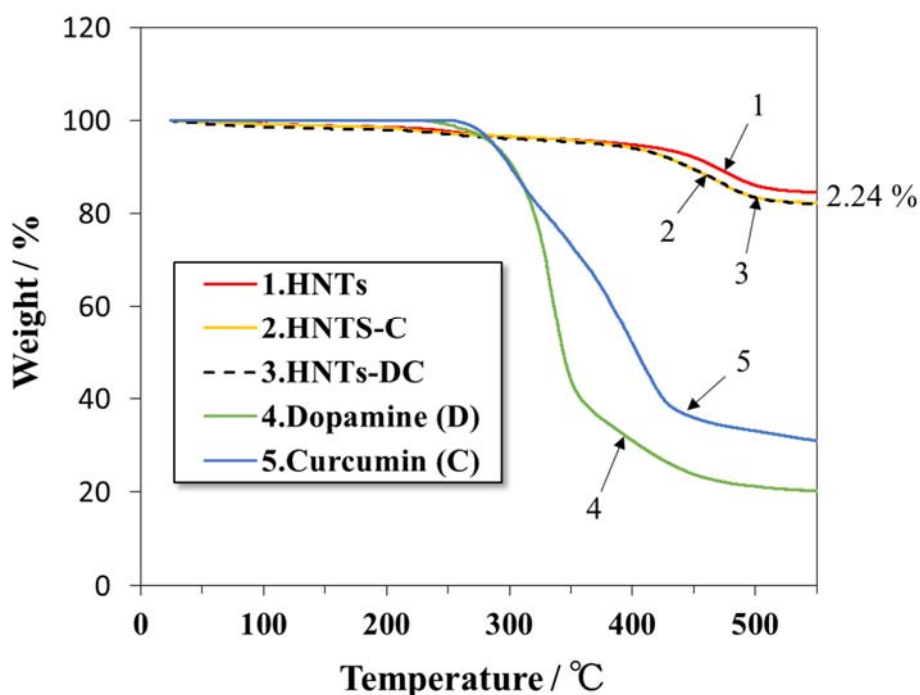
Figure 4-6. TG curves of HNTs (1), HNTs-C (2), HNTs-DC (3), Dopamine (4), and Curcumin (5).

4.3.4 Kinetics of the curcumin release

In vitro release of curcumin was investigated in the PBS and ethanol mixture solution by dialysis bag method. In case of pure PBS solution, curcumin did not come out of the dialysis bag. HNTs-DC, HNTs-C, free curcumin (FC), photo-crosslinked hyaluronic acid hydrogel encapsulating HNTs-DC (HA-HNTs) and FC (HA-C) was examined on their release in the different pH mixture solution of pH 7.4 and pH 5 for 48 hr.

FC was almost released into both the medium of pH 7.4 and pH 5.0 within 8 hr. At pH 7.4, HNTs-DC showed slower release than HNTs-C at initial level and sustained drug release during 48 hr (Figure

4-7). HNTs-DC showed the same release pattern regardless of the pH value during initial 6 hr, thereafter curcumin was released faster than pH 7.4 condition. Because Schiff base imine (C=N) is hydrolyzed easily at acidic medium than neutral conditions, it showed the faster release pattern (Figure 4-8). Curcumin is a hydrophobic material that is separated easily from the hydrophilic surface of HNTs. Curcumin is weakly attached on the outer surface and most of the amount was entrapped in the lumen of HNTs. Curcumin shows the fast release from the hydrophilic lumen of HNTs because it is weakly attached onto the aluminol groups of the lumen in case of HNTs-C. However, DC has a selectively reactive catechol groups, which has strong affinity onto the surface of aluminol groups. Dopamine has been reported to have a strong affinity to the aluminum surface. DC accumulated strongly onto the HNTs lumen. In neutral condition they are hydrolyzed slowly and detach, and also the tube structure hinders the diffusion of curcumin molecules. When the pH become lowers, DC detach easily from halloysite lumen because of the cleavage of C=N bond resulting in faster release.

To analyze the mechanism of drug release kinetics, in vitro drug release profiles was plotted in three mathematical models such as first order, Higuchi, and Korsmeyer-Peppas models (Figure 4-9, 4-10, 4-11 and Table 4-2,4-3,4-4).

First order : $\log (100 - Q) = \log 100 - k_1 t$ (4)

Higuchi kinetics : $Q = k_H t^{1/2}$ (5)

Korsmeyer – Peppas equation : $M_t / M_\infty = k t^n$ (6)

Where k_1, k_H, and k are drug release rate constants and Q is the percent of the released drug at time t. M_t / M_∞ is the fractional amount of released drug and n is the release exponent.
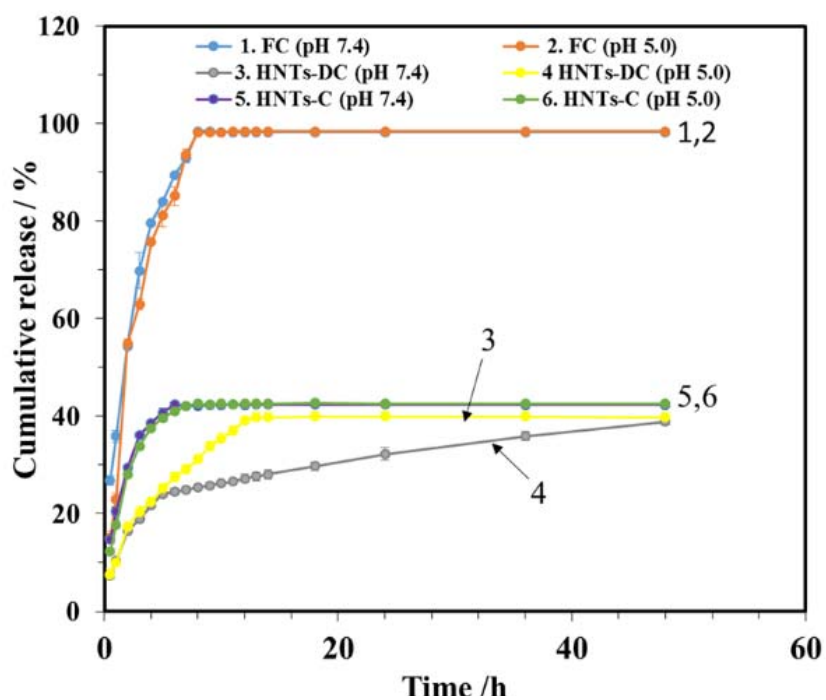
Figure 4-7. Curcumin release profile of free curcumin (FC), HNTs-DC, and HNTs-C at pH 7.4 and pH 5.0.
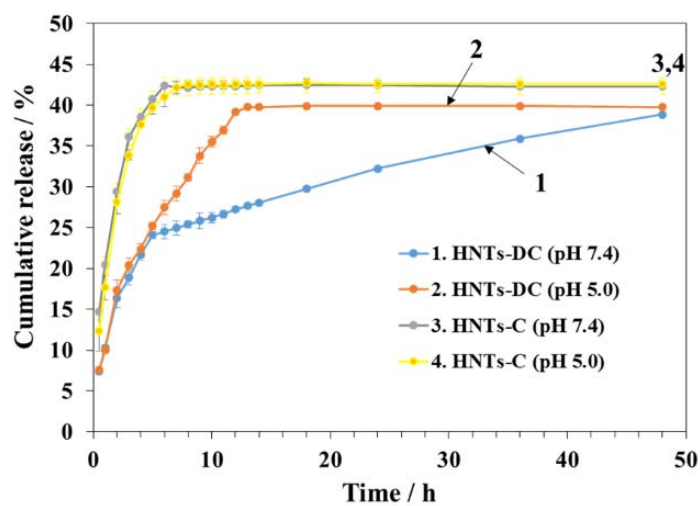
Figure 4-8. Comparison of curcumin release profile between HNTs-DC and HNTs-C at pH 7.4 and pH 5.0

Table 4-2. Release kinetic of FC

Release medium	First order		Higuchi		Korsmeyer-Peppas		
	k_1 (h^{-1})	R^2	k (h^{-1})	R^2	k (h^{-1})	n	R^2
pH 7.4	9.24	0.912	34.36	0.973	0.380	0.494	0.985
pH 5.0	10.63	0.900	39.57	0.996	0.214	0.773	0.983

Table 4-3. Release kinetic of HNTs-DC

Release medium	First order		Higuchi		Korsmeyer-Peppas		
	k_1 (h^{-1})	R^2	k (h^{-1})	R^2	k (h^{-1})	n	R^2
pH 7.4	2.34	0.862	8.86	0.971	0.106	0.483	0.982
pH 5.0	3.02	0.942	11.14	0.994	0.108	0.524	0.986

Table 4-4. Release kinetic of HNTs-C

Release medium	First order		Higuchi		Korsmeyer-Peppas		
	k_1 (h^{-1})	R^2	k (h^{-1})	R^2	k (h^{-1})	n	R^2
pH 7.4	3.48	0.801	13.37	0.913	0.207	0.416	0.972
pH 5.0	3.83	0.834	14.62	0.936	0.182	0.480	0.973
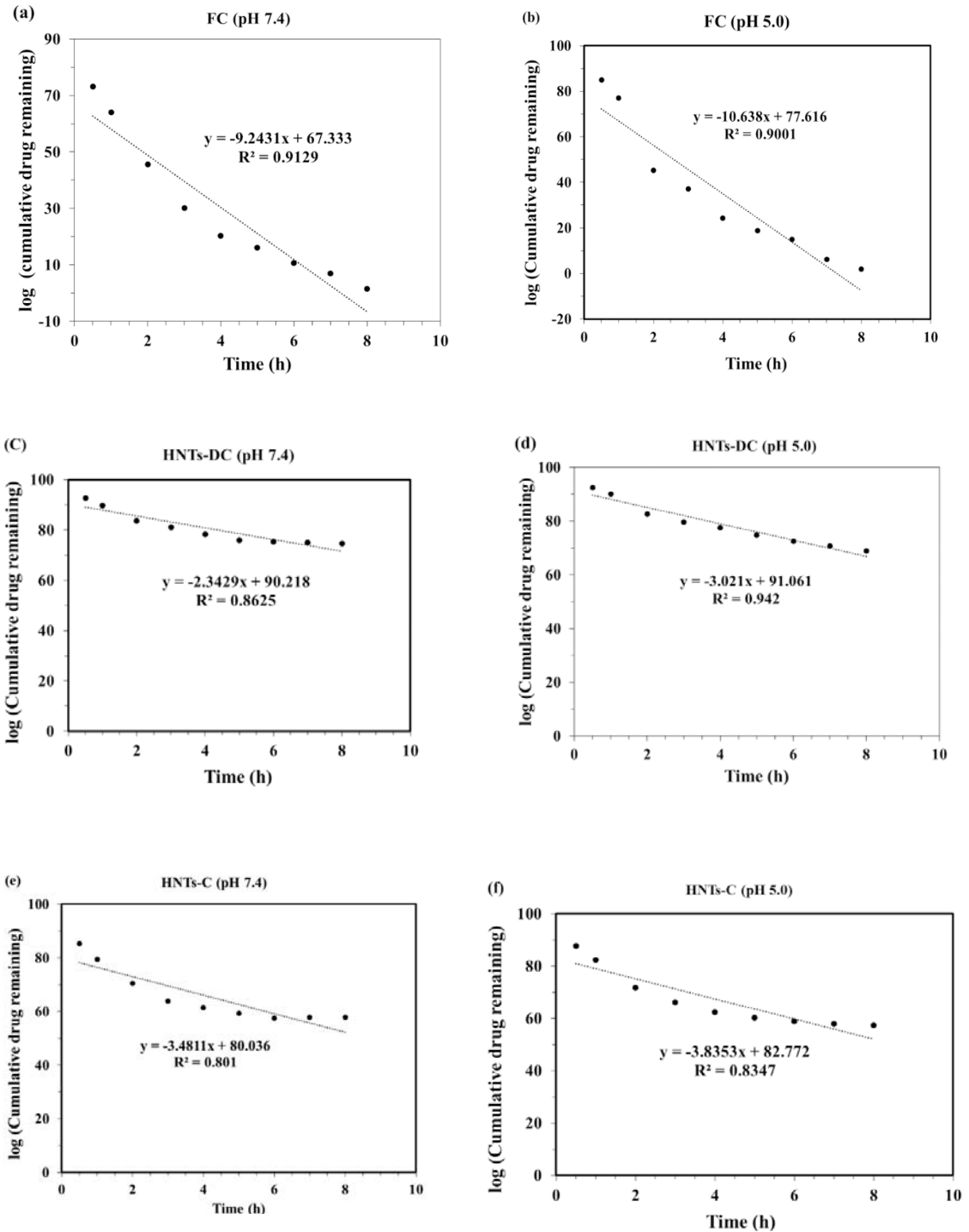
Figure 4-9. First order release kinetics of FC (pH 7.4) (a), FC (pH 5.0) (b), HNTs-DC (pH 7.4) (c),

HNTs-DC (pH 5.0) (d), HNTs-C (pH 7.4) (e), HNTs-C (pH 5.0) (d).
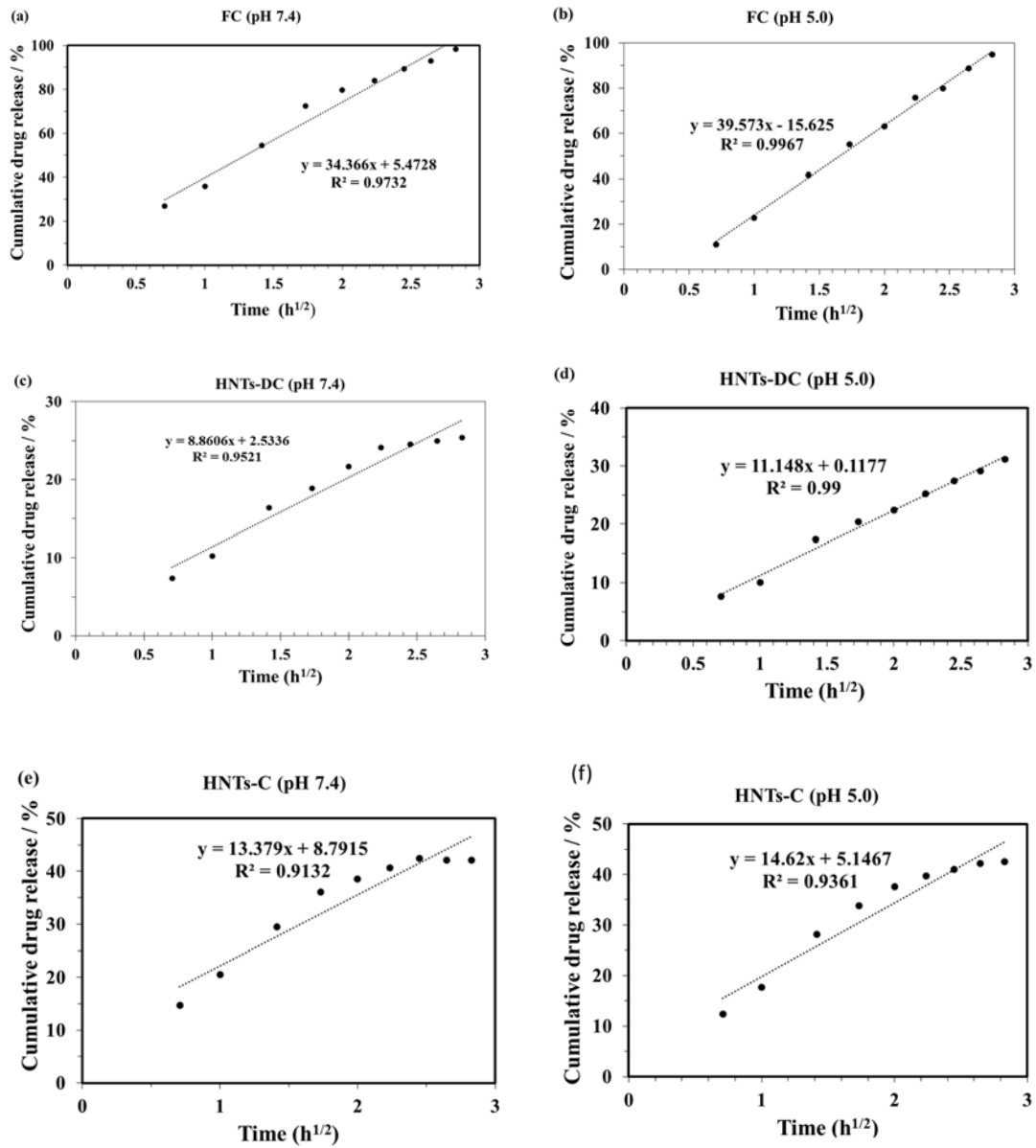
Figure 4-10. Higuchi release kinetics of FC (pH 7.4) (a), FC (pH 5.0) (b), HNTs-DC (pH 7.4) (c), HNTs-DC (pH 5.0) (d), HNTs-C (pH 7.4) (e), HNTs-C (pH 5.0) (d).
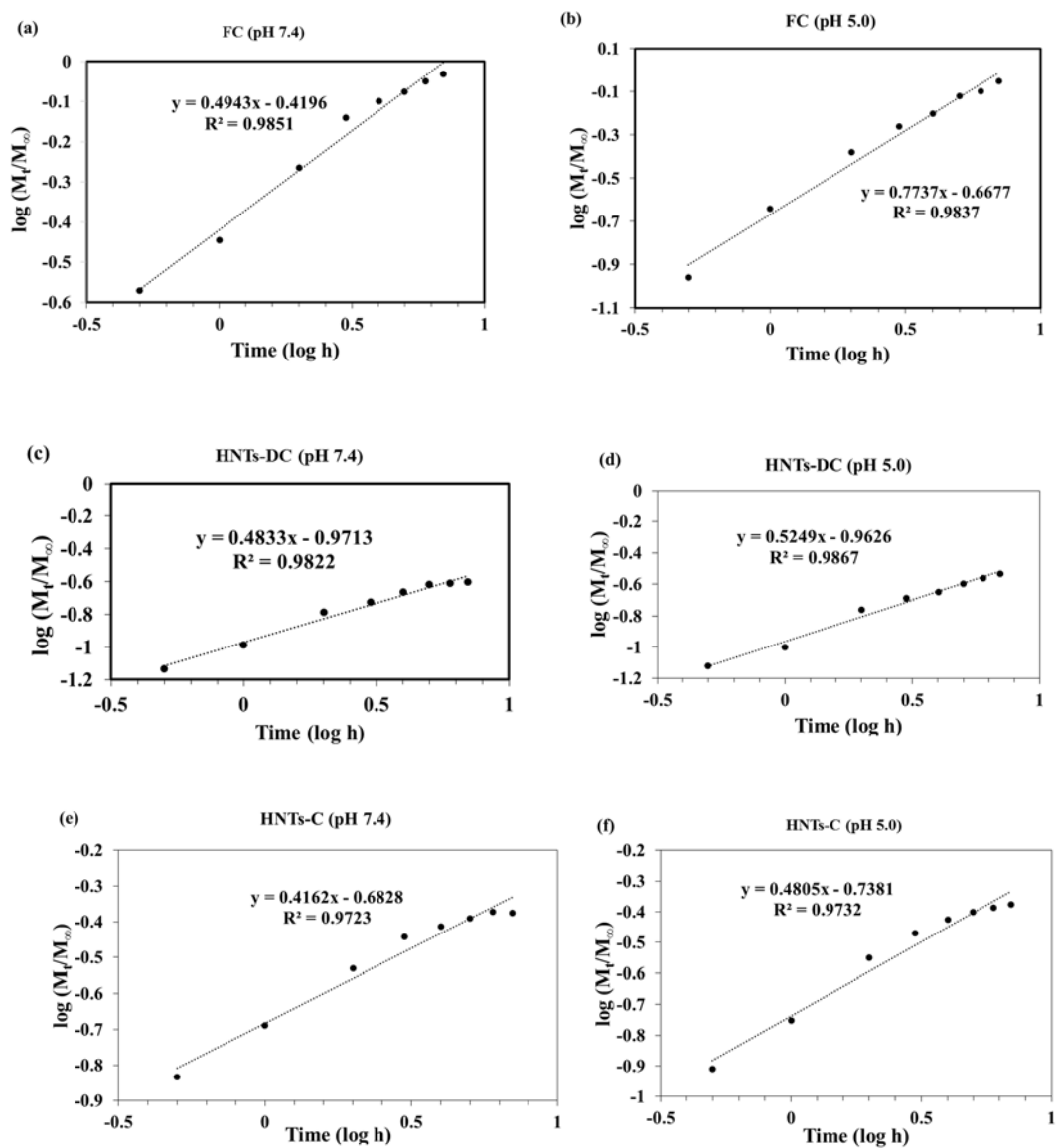
Figure 4-11. Korsmeyer-Peppas release kinetics of FC (pH 7.4) (a), FC (pH 5.0) (b), HNTs-DC (pH 7.4) (c), HNTs-DC (pH 5.0) (d), HNTs-C (pH 7.4) (e), HNTs-C (pH 5.0) (d).

The diffusion of drug release can be explained by either Fickian or non-Fickian. In Fickian diffusion, release rate is independent of the drug concentration. In non-Fickian diffusion, however, several factors can affect the drug release rate. The most ideal drug delivery mechanism with controlled release is a zero-order release in which a drug is released at a constant rate.

First order kinetic model describes absorption and elimination of certain drugs, which explains that the concentration with respect to time is dependent only on concentration. The fitted correlation coefficient (R^2) values of first order kinetics were very low for all the samples (Table 1-3). FC, HNTs-C and HNTs-DC followed the Higuchi and Korsmeyer-Peppas release kinetic mechanism during initial 9 hr because R^2 is almost the same in FC and HNTs-DC. FC has higher rate constant in both mechanism than HNTs-DC indicating faster release. In Higuchi and Korsmeyer-Peppas model, HNTs-DC at pH 5.0 has higher rate constant value than pH 7.4 indicating pH sensitive faster release behavior whereas HNTs-C did not show the pH sensitive release pattern, consequently it was released fast at any pH condition, and finally reached the equilibrium concentration fast as much as FC.

Higuchi model has the conditions such as : (a) the drug concentration in the matrix is initially much higher than the solubility of the drug, (b) drug diffusion takes place only in one dimension (edge effects are negligible), (c) the thickness of the dosage form is much larger than the size of the drug molecules, (d) the swelling and dissolution of the matrix is negligible, (e) the diffusivity of the drug is constant, (f) and perfect sink conditions are always attained in the release environment.[25] Higuchi model does not consider the swelling or contracting of the matrix, edge effect of the matrix and the pore formation or collapse during the release. Therefore, Higuchi equation is not appropriate to applied to the HNTs which has lumen and rolled structure that does not follow the Fickian diffusion. In case of the Korsmeyer-Peppas equation, the diffusion exponent n characterizes the transport mechanism and different release for cylindrical shaped matrices. The value of n less than 0.45 indicates the drug release

follows the Fickian diffusion of swelling-controlled system from cylindrical particles, whereas values in the range of $0.45 < n < 0.89$ corresponds to the non Fickian diffusion.[25-27] HNTs-DC has a value of 0.483 and 0.527 at pH 7.4 and pH 5.0, respectively which indicates that HNTs-DC was released in anomalous transport manner at both pH conditions. Curcumin from HNTs-DC at pH 5.0 was released faster in anomalous diffusion manner than pH 7.0 attributed to the factor of faster hydrolysis of imine bond.

Hydrogels encapsulating HNTs-DC showed the much slower release at the initial stage compared to the hydrogel containing the curcumin only (Figure 4-12). This can be explained that curcumin molecule in HA-HNTs should pass the multiple paths, i.e. halloysite lumen and polymer matrix. Moreover it should overcome the interaction with halloysite inner lumen and polymer chain. Thus, double barrier structure consisting of clay nanotube encapsulated within hydrogels, containing the drug molecules in- and outside the clay nanotubes, can contribute to the sustained drug delivery.
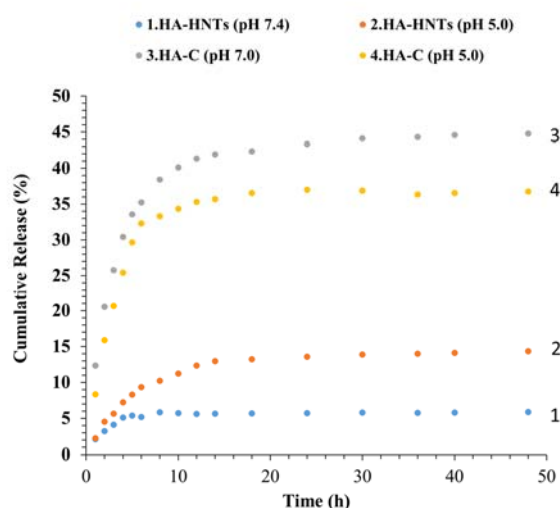
Figure 4-12. Curcumin release profile from HA-HNTs (1, 2) and HA-C (3,4) at pH 7.4 and pH 5.0

4.4 Conclusion

HNTs-DC are expected to be useful in sustained and controlled drug delivery system as a prodrug because it shows the pH sensitive behavior at lower pH. Curcumin combined to the dopamine by Schiff base reaction and the catechol group is selectively bond to the aluminol surface. It was encapsulated in the HNTs lumen and subsequently chemisorbed to the inner surface. This curcumin prodrug showed the sustained and controlled drug release because of imine bond cleavage at acidic condition, resulting in the pH sensitive curcumin release profile.

In the release kinetic analysis, HNTs-DC was fitted well with the Korsmeyer-Peppas release model. The release exponent was slightly increased at pH 5.0 which means the multiple release pattern was included. Curcumin from HNTs-DC at pH 5.0 was released faster than pH 7.0 attributed to the factor of faster hydrolysis of imine bond.

HNTs-DC showed sustained drug release compared to the free curcumin and simply curcumin loaded HNTs. HNTs-DC showed sustained curcumin release at neutral pH but it was released faster at acidic pH. HNTs-DC showed more sustained drug release when it is encapsulated in the hyaluronic acid hydrogel because of the increment of diffusion paths and interaction with the environment. This leads to the sustained drug release that is essential for tissue engineering.

References

[1] M. L. Zheludkevich, D. G. Shchukin, K. A. Yasakau, H. Möhwald, M. G. S. Ferreira, *Chem. Mater.* **2007**, 19, 402.

[2] Z. Zheng, M. Schenderlein, X. Huang, N. J. Brownbill, F. Blanc, D. Shchukin, *ACS Appl. Mater. Interfaces* **2015**, 7, 22756.

[3] J. Yang, J. Lee, J. Kang, K. Lee, J-S. Suh, H-G. Yoon, Y-M. Hugh, S. Haam, *Langmuir* **2008**, 24, 3417.

[4] Z. Luo, K. Cai, Y. Hu, L. Zhao, P. Liu, L. Duan, W. Yang, *Angew. Chem. Int. Ed.* **2011**, 50, 640.

[5] P. Broz, S. Driamov, J. Ziegler, N. Ben-Haim, S. Marsch, W. Meier, P. Hunziker, *Nano Lett.* **2006**, 6, 2349.

[6] J. Shang, G. Li, R. Singh, P. Xiao, J. Z. Liu, P. A. Webley, *J. Phys. Chem. C*, **2010**, 114, 22025.

[7] D. G. Sh D. G. Shchukin, H. Möhwald, *small*, **2007**, 3, 926.

[8] D. G. Shchukin, H. Möhwald, *Adv. Funct. Mater*, **2007**, 17, 1451.

[9] E. Shchukina, D. Grigoriev, T. Sviridova, D. Shchukin, *Prog. Org. Coat.* **2017**, 108, 84.

[10] Y. Lvov, E. Abdullayev, *Prog. Polym. Sci.,* **2013**, 38, 1690.

[11] D. G. Shchukin, S. V. Lamaka, K. A. Yasakau, M. L. Zheludkevich, M. G. S. Ferreira, H. Möhwald, *J. Phys. Chem. C* **2008**, 112, 958.

[12] M. Massaro, R. Riela, C. Baiamonte, J. Blanco, C. Giordano, P. Meo, S. Milioto, R. Noto, F. Parisi, G. Pizzolanti, G. Lazzara, *RSC Adv.* **2016**, 6, 87935.

[13] S. Wanninger, V. Lorenz, A. Subhan, F. T. Edelmann, *Chem. Soc. Rev.* **2015**, 44, 4986.

[14] K. I. Priyadarsini, *molecules*, **2014**, 19, 20091.

[15] J. Li, G. H. Shin, X. Chen, H. J. Park, *Food Res. Int*. **2011**5, 69, 202.

[16] W. Rao, W. Zhang, I. P-F. Y. Wang, Y. Lei, P. Agarwal, B. Weekes, C. Li, X. Lu, J. Yu, X. He, *Acta biomater.* **2014**, 10, 831.

[17] S. Wanninger, V. Lorenz, A. Subhan, F. T. Edelmann, *Chem. Soc. Rev.* **2015**, 44, 4986.

[18] I. Ali, A. Haque, K. Saleem, M. F. Hsieh, *Bioorg. Med. Chem.* **2013**, 21, 3808.

[19] W. A. Zoubi, A. A. S. Al-Hamdani, M. Kaseem, *Appl. Organometal. Chem.* **2016**, 30, 810-817.

[20] J. Donoso, F. Muñoz, A. A. García Del Vado, G. Echevarría, F. García Blanco, *Biochem. J*. **1986**, 238, 137.

[21] W. O. Yah, H. Xu, H. Soejima, W. Ma, Y. Lvov, A. Takahara, *J. Am. Chem. Soc.* **2012**, 134, 12134.

[22] Y. Liu, K. Ai, L. Lu, *Chem. Rev.* **2014**, 114, 5057.

[23] Y. Lin, C. Chen, C. Wang, F. Pu, J. Ren, X. Qu, Chem. *Commun.* **2011**, 47, 1181.

[24] S. Mondal, S. Ghosh, S. P. Moulik, *J. Photochem. Photobiol, B*, **2016**, 158, 212.

[25] J. Siepmann, N. A. Peppas, *Int. J. Pharm.* **2011**, 418, 6.

[26] M. M. Ayad, N. A. Salahuddin, A. A. El-Nasr, N. L. Torad, *Microporous Mesoporous Mater.* **2016**, 229,166.

[27] M. Liu, Y. Chang, J. Yang, Y. You, R. He, T. Chen, C. Zhou, *J. Mater. Chem. B*, **2016**, 4, 2253.

Chapter 5

Conclusions and perspectives

In this thesis, the physicochemical properties of two types of hybrid hydrogels were investigated. In Chapter 2, imogolite/hyaluronic acid hybrid hydrogels, prepared by adjusting the optimal pH, showed increased mechanical properties maintaining good swelling properties because hydrophilic properties of imogolite network make it possible to interact strongly with crosslinked hyaluronic acid networks. The effect of reinforcement on Imogolite/hyaluronic acid hydrogel was characterized by compressive mechanical test and dynamic oscillatory shear test. Imogolite/hyaluronic acid hydrogels showed enhanced strain at break and fracture stress, and effective energy dissipation and restoration when the stress was given.

In Chapter 3, through the surface modification of halloysite, halloysite network interacts strongly with hyaluronic acid network by covalent bonds to overcome the repulsive interaction between them. The mechanical properties of halloysite/hyaluronic acid hydrogels were optimally adjusted by the content of halloysite amounts. The excessive amount of halloysite reduced the mechanical strength because of the aggregation of halloysite resulting in the formation of numerous void of network structure.

In Chapter 4, halloysite nanotubes showed the sustained and controlled drug release through pH-stimuli responsive properties. Curcumin was functionalized with dopamine by Schiff base reaction and it was selectively reacted to the halloysite nanotube lumen. This prodrug showed the sustained and controlled drug release at acidic condition.

Bioactive molecules rapidly diffuse out of hydrogel polymer networks when they are simply dispersed within the gels without any covalent or non-covalent interactions, resulting in the fast release. Bioactive molecules entrapped inside the micro- or nano- particles have to diffuse through two barriers, i.e. particle vehicles and hydrogels to be released into surrounding media, which can reduce burst release effect and prolong the release duration. Hybrid hydrogels have been used to modulate the

release of small molecule drugs, genetic material, proteins, and vaccines. These systems also allow multiple delivery of different bioactive agents with independent release rates.

Aluminosilicate nanotubes can be not only a potential drug delivery device but also biological nanocomposite scaffolds component for therapeutics and tissue engineering repair. Because of their high surface activity and intrinsic nanotube structure, multifaceted nanocomposite materials can be kept developing in other industrial area as well as biomedical applications.

Acknowledgements